2016

Unstructured-grid model for the North Sea and Baltic Sea: Validation against observations

Yinglong J. Zhang
Virginia Institute of Marine Science

EV Stanev

S Grashorn

Unstructured-grid model for the North Sea and Baltic Sea: validation against observations

Yinglong J. Zhang[a1], E.V. Stanev[b], and S. Grashorn[b]

a.Virginia Institute of Marine Science,
College of William & Mary,
Center for Coastal Resource Management,
1375 Greate Road,
Gloucester Point, VA 23062,
USA
b. Institute of Coastal Research,
Helmholtz-Zentrum Geesthacht
Max-Planck-Str. 1
21502 Geesthacht
Germany

[1] Corresponding author; e-mail: yjzhang@vims.edu; phone: (804) 684-7466; fax: (804) 684-7179.

Abstract

A new unstructured-grid model and its application to the North Sea and Baltic Sea are described. The research focus is on the dynamics in the two basins and in the multiple straits connecting them and more specifically on how the model replicates the temporal and spatial variability of physical processes. The comparison against observed data indicates the realism in the simulations of the exchange flows. The simulations demonstrated that in contrast to the tidal variability which decreases in the strait, the role of the barotropic forcing due to weather systems increases. In this zone reversal of transport is well manifested by the increased difference between the surface and bottom salinity values. Small sub-basins like Arkona and Bornholm play the role of reservoirs for denser water which under specific conditions cascades on its way to the Gotland Deep. Unlike the intermediate and deep water salinity in the Baltic Sea, which is strongly affected by fluxes in the straits, the simulated winter-refill and evolution of cold intermediate water are rather driven by surface cooling and processes in the upper mixed layer.

Key words: SCHISM; ocean circulation; strait processes; temperature; salinity/density; North Sea; Baltic Sea

1. Introduction

The North Sea and Baltic Sea (Fig.1) represent coupled tidal and non-tidal basins of approximately equal size connected through a system of straits. This straits system (hereafter the North Sea - Baltic Sea Transition Zone (NBTZ)) includes the Kattegat, Danish straits and the western part of the Baltic Sea. The surplus of fresh water in the Baltic Sea and the limited water exchange with the North Sea support a two-layer exchange flow in the NBTZ and explains the low salinity (brackish water) of the Baltic Sea. The deep part of the Baltic Sea known as the Baltic proper is separated from the straits area by a number of sills: the Darss Sill (depth of 18m), the Drogden Sill (depth of 8m) and the Stolpe Channel (depth of 63-64 m) further east. In these shallow areas the inflowing North Sea water is subjected to substantial mixing with the highly stratified Baltic Sea water.

The North Sea - Baltic Sea system represents a challenge for the numerical modelling because of several reasons. The first one is that it consists of a tidal and non-tidal basin with different dominating balances in each individual basin. The tidal one (the North Sea) is very shallow, except for the Norwegian trench. The relatively high salinity values in the North Sea are typical for the ocean; the vertical mixing which is mostly due to tides dominates the hydrophysical fields. The second basin (the Baltic Sea) can be considered as a huge estuary with extremely strong vertical stratification, which inhibits the vertical mixing. The diffusion coefficients approach to their molecular values, resulting in the extremely weak mixing between the surface and deep layers. This specific vertical stratification is maintained by two major factors: (1) the river runoff and precipitation-evaporation balance at sea surface, and (2) periodic intrusions of saltier North Sea water triggered by extreme atmospheric conditions with an approximately decadal periodicity.

The second challenge in the modelling of Baltic Sea and the area of Skagerrak and Norwegian Trench stems from the fact that the processes there are strongly dependent upon the exchanges in the NBTZ. Compared to other similar transition zones (e. g. Mediterranean – Atlantic Ocean or Black Sea – Mediterranean; Sannino et al., 2009, Stanev and Lu, 2013), the NBTZ is more complex because of the presence of multiple straits. Under different weather or circulation conditions their individual contribution to the exchange between the basins varies (Stanev et al., 2015). Thus the partitioning of flows and recirculation in the belts (which includes 3 major waterways: Great Belt, Little Belt, and Oresund) are central to the problem of the ventilation of deep Baltic basins by the North Sea water (see also, Meier, 2005; 2007). Extremely high resolution is needed there in order to resolve the complex coastal line as well as the bottom topography found in the three straits (note that the Little Belt is only 1 km wide). Without an adequate resolution the hydrodynamics of the inflow-outflow system cannot be accurately simulated.

A number of numerical models based on primitive equations and finite-difference discretization have been used to simulate the circulation in the coupled North Sea – Baltic Sea; e.g., models of Funkquist and Kleine (2007), She at al. (2007), Fu et al. (2011; 2012), Zhuang et al. (2011). More detailed references are given in Meier and Kauker (2003), Lehmann et al. (2004), Schmidt et al. (2008), Leppäranta and Myberg (2009). However the horizontal resolution in these models did not allow sufficient resolution in the three straits. Burchard et al. (2005; 2009) used a

horizontal resolution of 0.5 nm to study the dominant dynamics in the Western Baltic Sea and validated the model performance with a focus on the mixing in the areas of Drogden Sill, Darss Sill and the Bornholm Channel. Although this resolution was not sufficient for the Sound and inadequate for the Little Belt, the idealized simulations of the authors allowed determination of the pathways of salt transport during medium-intensity inflow events (see also Meier, 2007), demonstrating a reasonable consistency with the observations. However in these publications some problems with the open boundary conditions at the Kattegat, and also with the initialization strategy have not been resolved; e.g., forced with the climatological condition, the model did not fully recover this condition in an annual simulation (Meier, 2007).

Motivated by the above challenges we (1) address the resolution problem by enabling sufficient resolution in the straits, and (2) avoid inconsistencies in some earlier studies. Some of these inconsistencies are associated with either the forcing being prescribed in the NBTZ, or with the one-way or two-way nesting techniques, which are not seamless. Therefore we describe in the present paper an application of an unstructured-grid model for the coupled basins starting from the English Channel in the South up to the Shetland Islands to the North. This configuration enables the seamless propagation of the large-scale forcing into the NBTZ (see Danilov, 2013 for a review of recent developments and practices on using unstructured meshes in ocean modelling and for more references). Unlike other applications of unstructured models for this region (e.g. Kliem et al. 2006), we use a 3D baroclinic set up. This presents a third challenge because it has never been shown before how unstructured-grid models can adequately simulate the complex thermohaline structure of two basins. If the adequacy is demonstrated, the model could be used also for other similar ocean areas.

It's our hope that our research will shed new light on the pros and cons of the current model vs other more traditional models (including both structured- and unstructured-grid models). The major differences include: implicit time step (which avoids splitting errors and enables efficiency and robustness), and treatment of momentum advection with Eulerian-Lagrangian Method (ELM, which further boosts efficiency and robustness) (although central-difference scheme has also been implemented). While the use of Galerkin Finite Element Method (GFEM) is not new, the combination of it with the previous two features seems to have achieved a good balance in terms of numerical diffusion and dispersion, as the numerical diffusion inherent in an implicit method and ELM is balanced out by the numerical dispersion inherent in GFEM. This is very

different from other earlier finite-volume models such as ELCIRC (Baptista et al. 2005) where numerical diffusion is dominant (another major advantage in this regard is SCHISM's ability to handle very skew elements and be completely free of orthogonality constraint). As a result, the model can be effectively used to simulate cross-scale processes with both accuracy and efficiency. However, as an unstructured-grid model, it's not immune to some common issues such as sensitivity to grid generation. The latter does not have an easy answer as the quality of model results is clearly tied to the grid used, and while there are some generic guidelines about mesh quality, ultimately the issue is application dependent. We are in the process of carefully testing and documenting this issue for a variety of barotropic and baroclinic applications including baroclinic instability (eddies and meanders), and comparing our results with those from structured-grid models (Zhang et al. submitted).

The research questions and novelties can be briefly summarized as follows.

1. Describe a new model and its application to a very specific region, which is dominated by tides and shelf processes, baroclinic processes driven by fresh water fluxes in the Baltic Sea and very specific (shallow) transition zone. Addressing all these needs good quality of simulation of both barotropic and baroclinic processes.
2. Quantify how well the model replicates the temporal and spatial variability of physical processes in the studied area.
3. Make available a reproducible reference set-up for this model to be used in further studies.

While deeper analysis of processes will be addressed elsewhere, this paper is focused on validating the new model. In section 2 we describe the model used. Section 3 describes the dynamics of sea level and the inter-comparisons with observations. Section 4 addresses the simulations of thermohaline fields, and Section 5 describes the quality of simulations of water mass structure. Short conclusions are formulated at the end. Because the processes in the two basins differ greatly, the validation presented here is not fully symmetric for the two basins; the baroclinic part of the Baltic Sea is presented in more detail along with the issue of water mass structure.

2. The model

2.1 Model description

SCHISM (Semi-implicit Cross-scale Hydroscience Integrated System Model; Zhang et al. submitted) is a derivative product of the original SELFE model (Zhang and Baptista 2008), with many improvements implemented by the first author at College of William & Mary and collaborators. It solves Reynolds-averaged Navier-Stokes (RANS) equation with transport of heat, salt and tracers in the hydrostatic form with Boussinesq approximation, using unstructured grids. Due to its highly flexible framework the model has found a wide range of cross-scale applications worldwide, from creeks to deep oceans: general circulation (Zhang et al. 2015), storm surges (Bertin et al. 2014), tsunami hazards (Zhang et al. 2011), water quality (Wang et al. 2013), oil spill (Azevedo et al. 2014), sediment transport (Pinto et al. 2012), and biogeochemistry (Rodrigues et al. 2009). The model is being distributed as an open-source community-supported model under an Apache license (http://www.schism.wiki).

New development since the last writing (Zhang et al. 2015) includes: addition of mixed triangle-quadrangles grid, and 1D/2D/3D options all wrapped in a single model grid. These new additions greatly extend the capability of SCHISM and have been reported in Zhang et al. (submitted).

Currently no ice model is available within the SCHISM system, and this may explain some errors near the Bay of Bothnia.

2.2 Description of the numerics

SCHISM solves the hydrostatic RANS and transport equations using a hybrid Finite Element and Finite Volume approach grounded on unstructured grids in the horizontal dimension. The efficiency and robustness of SCHISM are mostly attributed to the implicit treatment of all terms that place stringent stability constraints (e.g. CFL) and the use of Eulerian-Lagrangian method for the momentum advection. The vertical grid has recently been extended from the original *SZ* (i.e. partially terrain-following *S*- and partial *Z*-coordinates) to a highly flexible LSC^2 (Localized Sigma Coordinates with Shaved Cell) grid. Zhang et al. (2015) demonstrated the superior performance of LSC^2 in cross-scale applications. LSC^2 is also applied in the current study and we'll demonstrate its capability to maintain sharp stratification in the Baltic Sea (cf. Fig. A1).

2.3 The model grid

Fig. 2a shows the grid size distribution of the unstructured grid covering North Sea & Baltic Sea. Altogether there are ~300K nodes and ~600K triangles, with some refinement along the German Bight and Danish straits, where a nominal resolution of 200m is used (Fig. 2b), with the minimum grid size of 60m found in the narrow Little Belt. Some comparison studies were conducted using two types of vertical grids supported by SCHISM: (1) 31 *S* levels with stretching constants of θ_b=1, θ_f=4 (Zhang and Baptista 2008); (2) an LSC^2 grid with a maximum of 59 levels and an average of 29 levels in terms of computational cost (Zhang et al. 2015). The adoption of LSC^2 grid clearly has led to superior results especially in terms of stratification in the Baltic Sea (Fig. A1 in Appendix 1), and so this is the vertical grid used below. More examples of LSC^2 results can be found in Zhang et al. (2015).

2.4. The model forcing

On the open North Sea boundaries (Scottish Shelf and English Channel) time series of elevation, horizontal velocity, salinity and temperature are interpolated from MyOcean product (http://www.myocean.eu; last accessed in Jan 2015). The sea-surface boundary conditions use the output from the regional model COSMO-EU (wind, atmospheric pressure, air temperature and specific humidity) operated by the German Weather Service with a horizontal resolution of 7 km. Heat fluxes (including solar radiation and downward long wave (infrared) radiation) used come from NOAA's CFSR product (http://www.ncdc.noaa.gov/data-access/model-data/model-datasets/climate-forecast-system-version2-cfsv2; last accessed in Jan 2015). Monthly flow data at 33 rivers in the region are provided by the German Federal Maritime and Hydrographic Agency (Bundesamt für Seeschifffahrt und Hydrographie, BSH). Bathymetry data have been compiled from data provided by BSH, Danish Meteorological Institute and Baltic Sea Hydrographic Commission, 2013, Baltic Sea Bathymetry Database version 0.9.3 (http://data.bshc.pro/, accessed on June 5, 2015). No bathymetry smoothing is done in our computational grid.

2.5 Initialization and parameters

The model is initialized with zero elevation and velocity, and the 3D profiles of temperature and salinity from the climatological data of Janssen et al. (1999). The heat exchange model inside SCHISM is Zeng's (1998) bulk aerodynamic model. We use a constant albedo of 0.06 and a Jerlov type III water (Paulson and Simpson 1977) for light attenuation. As this paper concerns large-scale process, we use a constant bottom roughness value of 0.5mm without any fine tuning. The turbulence model used in this paper is *k-kl* (Umlauf and Burchard 2003), with a background diffusivity of 10^{-6} m^2/s.

A time step of 120s is used in the simulation which translates to a maximum CFL number of 16.7 (found in the NBTZ and some parts of the Norwegian North Sea coast). The transport of salinity and heat is done using a 2^{nd}-order TVD method for depths deeper than 8m, and a more efficient upwind method for shallower depths (i.e., the limiter functions are zeroed out for shallower depths); the finer resolution used in shallow-depth areas effectively mitigates the numerical diffusion in upwind method. The simulation period presented in this paper is from July 1, 2011 to Nov. 13, 2012, or 500 days in total.

2.6 Overall model computational performance

The simulations were conducted on Sciclone cluster of College of William & Mary (http://www.hpc.wm.edu/SciClone/Home; last accessed in Jan 2015), NSF's Stampede, as well as NASA's Pleiades. On 144CPUs of Sciclone, it runs ~180 times faster than real time. About 30% faster performance was achieved on the other two clusters.

3. Sea level

There are some important differences and similarities between the dynamics of sea level in the North Sea and Baltic Sea. In the North Sea the range of tidal oscillations is from more than 9 m in the English Channel to ~20 cm in the Kattegat. The narrow Danish straits damp the tidal oscillations and they propagate with measurable amplitudes no further than the Belts. The two basins, the North Sea and the Baltic Sea are in most of their areas shallow basins and therefore the atmospheric forcing creates a strong barotropic response. In the NBTZ the direction of the barotropic pressure gradient alternates (from/to the Baltic Sea), which is accompanied by a flow

reversal in the straits. In contrast to the deep parts of the Atlantic Ocean and the other two semi-enclosed European seas (the Black and Mediterranean Seas) the winter anomalies of sea level are positive in the shelf seas (Baltic Sea and northwest of European shelf) and negative in the deep basins (see Fig. 5.3 of Stanev and Lu 2013). This reflects the specific appearances of the fresh water budget, surface momentum and heat fluxes.

Because the variation of sea level in the North and Baltic seas are of utmost importance for the complex physical processes there and because their adequate simulations could guarantee the realism of interpretation of simulations, extensive validation of numerical simulations against tide gauge data has been performed. In the following we will focus on some specificity of sea-level dynamics in the both basins, as well as in the NBTZ. The latter zone is of particular importance not only because tidal amplitude reduces strongly (this is known for a long time) but also because tidal pumping can play the role of a possible driver affecting the straits exchange (Feistel et al. 2003b). Bendtsen et al. (2009) found that the tidal mixing was primarily concentrated to shallow areas around Kattegat and in the Great Belt. However these authors focused only on the NBTZ prescribing the tidal conditions at its boundaries. Furthermore, the horizontal resolution of their model was 2′×2′ minute and 30 vertical sigma layers, which is much coarser, compared to the resolution in the present study, thus justifying the revisit of this modelling issue using a coupled North Sea-Baltic Sea model with a very fine resolution in the straits.

3.1 The North Sea

The numerical simulations reveal the well-known anti-clockwise rotation associated with the Kelvin waves. The simulated tidal range reaches ~9m in the English Channel. One representative illustration of the spring-neap tide modulation is shown in Fig. 3a for the station of Jersey (Fig.1). At other stations, such as Helgoland this modulation is much less pronounced (Fig. 3b).

The Taylor diagram (Fig. 4) demonstrates in a systematic way the model skill. Most of the North Sea stations cluster in a small vicinity close to the purple star representing the “perfect model-performance”. While the correlation coefficient of all analyzed stations is 0.89 the ones in the North Sea (black dots in the Taylor diagram) show much better correlation. The model skill measured as the ratio between RMSE and the standard deviation of observation is about 0.1 (the

same number for all analyzed stations is 0.19). The deviations from this good performance at some stations may be associated with some dubious outliers in the observations.

3. 2 The Baltic Sea

The variability of Baltic Sea level is represented in Fig. 3 at the stations of Tejn, Kronstadt and Kemi. The first station is in the Bornholm Basin, the second is the eastern-most part of the Gulf of Finland and the third on the Finish coast in the Bothnian Bay (see Fig. 1 for their positions). In all three stations the temporal variability in the simulations agrees well with that in the observations; the response to the atmospheric forcing very clearly demonstrates that the latter governs the ocean variability. However the correlation between the individual stations is not particularly strong in either model or observations, indicating large differences in the regional responses. At the three stations the model slightly overestimates the amplitudes associated with the weather systems, in particular during periods of extreme winds, e. g. at day 75 in Fig. 3d. At Kronstadt the high-frequency basin modes are underestimated while at Tejn the amplitudes of basin modes are comparable with the observed values. The variability in the Bothnian Bay which is in the northernmost part of the Baltic Sea also demonstrates large wind driven response (Fig. 3e).

The overall skill of the model to predict the variability of sea level in the Baltic Sea is quantified by the blue circles in Fig. 4. In most of the stations the correlation coefficient is about 0.95; the scaled difference between model and observations is about 0.20. The model slightly over-predicts the range of oscillations. The performance is not satisfactory at Tallinn where the correlation with observation is ~0.72. Maximum over-predictions of the range of oscillations appear at Soru, St Petersburg and Tallinn, which are coastal locations in the Gulf of Riga and Gulf of Finland, possibly due to local bathymetric errors and or bottom friction. Note that the bathymetry used may not have fine enough resolution in many parts of Baltic. More detail about the quality of model performance is given in Appendix 2 where time series are shown exemplarily for 44 tide gauge stations around the Baltic Sea coast.

3.3 The NBTZ

The variability in the Danish straits is represented below with two stations: Kattegat (Frederikshavn, which is close to the North Sea boundary of the NBTZ) and Drogden which is at the southern entrance of the Sound (see Fig. 1 for their positions). Although very small (amplitudes less than 20 cm) the tidal oscillations in Frederikshavn are clearly pronounced (Fig. 3f). However unlike most stations in the open part of North Sea (Fig. 3a&b) their modulation does not reveal a clear spring-neap cycle, but is rather dependent on the meteorological conditions (weekly to 10-days oscillations are very clearly seen in Fig. 3f).

The tidal signal is substantially reduced on the other side of the Baltic Sea straits (Drogden). As seen in Fig. 3g, the tidal amplitudes there reach ~10 cm, but change strongly over time. The model replicates well all substantial oscillations seen in the observations; the range of oscillation reaches ~1m at times. The difference between Fig. 3f and Fig. 3g also indicates very strong amplitudes and is instructive for the barotropic driving force in the straits, mostly due to the atmospheric forcing. The temporal evolution of sea level in Fig. 3c and Fig. 3g looks qualitatively more similar than between Fig. 3f and Fig. 3g. The most pronounced difference between Fig. 3c&g is the further reduction of the tidal range as one approach the Baltic proper.

At most of the stations in the NBTZ presented in Fig. 4 (red circles) the correlation coefficients are about 0.9, but there are some stations with the correlation < 0.9. At some stations the model over-predicts the variability (e. g. the normalized RMSE is relatively high at Fredericia).

The contrast between the points in the three different areas in Fig. 4 demonstrates that the straits are the most difficult part to simulate correctly even with the high resolution used here. However, the temporal evolution of sea level presented in Appendix 2 demonstrates that the overall performance of the model is good also in the NBTZ. Note that some ‘errors’ are due to some suspicious outliers in the observations, which remained in the validation data set despite our effort to eliminate obvious outliers; Fig. A2 shows some of these suspicious data at some stations. We did not filter out those data because their quality is dubious.

4.Thermohaline fields.

4.1 Surface-to-bottom salinity difference in the shallow channels of the NBTZ

The temporal change of surface-to-bottom salinity difference is very instructive for the regime of vertical mixing and re-stratification. The numerically simulated temporal variability of salinity in the Fehmarn Belt matches relatively well the similar variability seen in the observations (Fig. 5). The skill of the model is quantified by the RMS errors normalized by the standard deviations of observation: 0.18 at the surface and 0.18 at the bottom layer (the non-normalized RMS errors are 2.03 and 1.68; the standard deviations of observation are 11.27 and 9.34, respectively). The normalized model biases are 0.16 (surface) and 0.16 (bottom). The correlation coefficients are 0.80 (surface) and 0.76 (bottom), and the Wilmot scores (Wilmot 1981) are: 0.82 (surface) and 0.72 (bottom).

The maximum salinity up to 22 occurs in winter when the vertical stratification is weak. The stratification disappears during 1-2 months, with the sea-surface salinity (SSS) reaching ~20 (compare also with Feistel et al., 2003a; Feistel et al., 2006). Both the model and the observations clearly showed several small outflow events revealed by the decrease of salinities with weakly time scales (e. g. between days 187 and 194 in Fig. 5). Although the model does not exactly replicate these events, their phase and duration agree well with the observations. The outflow-dominated conditions are well illustrated by the increased difference between the surface and bottom salinity values during days 120-150. This difference decreased dramatically by the end of fall (day 150), which is interpreted as a result of the vertical mixing due to cooling from the atmosphere, which changes the properties of waters entering the straits from neighboring basin. During such conditions the outflow signatures of salinity are a combination of variability with weekly periods, which is triggered by meteorological forcing and small short-periodic oscillations over-imposed.

4.2 Temporal evolution of salinity and temperature in the Arkona Basin

The penetration of mixed North Sea water into the Baltic Sea follows a pathway along channels, sills and small deeper basins such as the Arkona and Bornholm Basin (Jakobsen 1995). The latter two basins play the role of reservoirs for denser water which under specific conditions propagates to the next (deeper) basin on their way to the Gotland Deep. Therefore it is worthwhile to analyzing the simulation results in these basins.

With the increasing distance from the straits, the inflow increasingly resembles the gravity flows (Fig. 6b, d). During most of the time the dominant two-layer salinity stratification is very clear both in the observations and simulations: about 5-10 m thick saltier bottom layer with salinities of ~14-18 is overlain by a thicker surface layer with salinity less than 8. Although the simulations appear slightly more diffuse than the observation and the bottom salinity is slightly overestimated, the timing of the individual bottom salinity maxima matches well, suggesting that the individual inflow events are captured by the model.

We remark that Fig. 6 displays more than four months of data during the summer and fall of 2012. At the beginning of this period (summer) the cold intermediate layer (CIL) is very pronounced with an axis at ~30-35 m reaching at some times the bottom at the analyzed location (Fig. 6 a, b). The model produces slightly weaker vertical stratification, and the depth of the thermocline is ~5m too shallow; this indicates an overall reasonable model performance. The cold water content is reduced several times due to strong warming from above. After the day 435 this layer collapsed, as seen in the observations and numerical simulations, as a result of the inflow of warm and high-salinity surface water from the straits. After day 460 (i.e., fall) the depth of surface cooling increases, and the upper layer is cooled more than the bottom. However the strong salinity stratification of deeper layer (Fig. 6 c, d) does not allow a complete mixing of the entire water column.

The correlation coefficients between simulated and observed temperature and salinity are 0.87 and 0.77, respectively. Although the RMSE and bias for the bottom salinity seem relatively large (1.35 and 0.97 PSU, respectively), it is small compared to the standard deviation of data (6.8 PSU), demonstrating a good skill.

The large differences between presented simulations and observations are explained by the large contrasts in the NBTZ and their rapid changes. However in comparison with other estimates they are not so large. For example, Fu et al. (2012) reported a salinity bias of plus 3-4 psu in the Bornholm Basin. In contrast to the present study these authors used data assimilation. In a similar study Liu et al (2013) demonstrated that compared to the free run, temperature and salinity had been improved significantly with data assimilation. Our results demonstrate that there is still a potential to get reasonable results even without data assimilation if more adequate resolution in the NBTZ is used.

4.3 The Sea Surface Temperature (SST)

Recall that the thermohaline part of the model forcing includes heat and water fluxes. In the following the Operational Sea Surface Temperature and Sea Ice Analysis (OSTIA) data will be used as the validation data set. The OSTIA system produces a high resolution analysis of the current SST for the global ocean using satellite data provided by the GHRSST (The Group for High-Resolution SST) project, together with in-situ observations to determine the sea surface temperature (Donlon et al., 2009). The analysis was performed using a variant of optimal interpolation described by Bell et al. (2000) and is provided daily at a resolution of $1/20^{o}$ (~5km).

The comparison between OSTIA and model results is presented in the following for simulation days 30-500. The RMSE between model and OSTIA data is small over most of the North Sea (less than 1^{o}C) (Fig. 7a). The low-error zone extends from the northern open boundary to the south mostly following the western coast. The simulations in the English Channel show errors reaching locally ~1.5 ^{o}C, which is mostly due to some boundary condition errors there (note some large errors right at the boundary). The comparison with the range of temperature fluctuations in this region demonstrates that the relative errors are small. The local maximum in the northeastern part of the basin is due to errors in OSTIA data (which can be seen from the fact that the SST from OSTIA there is mostly stationary over time). However the larger errors in the western part of Skagerrak and along the Norwegian Trench could present a motivation to further improve the performance of the model in these areas. It's encouraging that the errors in NBTZ are generally small.

The RMSE pattern in the Baltic Sea could give a possible explanation of the large differences between the simulation and observation in the Skagerrak. High errors occur usually along the west coasts of Baltic Sea and south of them. In this neighborhood OSTIA data are sometimes unavailable (see the blank zones). Upwelling events along the Swedish coast explain the substantially cooler temperatures than in the interior and southern part of the basin. The accompanied tilting of isotherms toward the Swedish coast and upwelled CIL there are clearly seen in the model results also (not shown). Therefore the bias in these areas is clearly negative (Fig. 7b). Other potential error sources include the lack of an ice model (especially for the Bay of Bothnia), or the wind stress parameterization.

5. The Water Masses

The question of whether or not the simulated water mass structure is correct under the variable horizontal resolution as found in unstructured grids is a critically important issue to be addressed when estimating the performance of a new (unstructured-grid) model setup for such a complex area. In the following 3 subsections, three aspects of this issue will be analyzed using the example of the formation of CIL, the two-layer exchange in the NBTZ and the propagation of bottom water into the Gotland Basin.

5.1 The Cold Intermediate Water

The vertical stratification in the Baltic Sea is dominated by salinity (Fig. 8b), which provides enormous stability, decreases vertical diffusion (Stigebrandt, 1987; Meier, 2001; Stanev, 1997; Omstedt, 2014) and therefore prevent the permanent halocline from being destructed by the winter cooling. The vertical salinity gradient at ~150 m only changes slightly, mostly in winter, as a result of the convective cooling. The small-scale oscillations at the interface, separating surface and deep waters, reveals the model representation of the oscillations of pycnocline.

The cold water mass formation starts in fall, first in a shallow part of the upper layer (Fig. 8a); in January-February the cooling reaches depths of ~60 m. This value varies in space reaching in some areas depths of ~65 m. The 25 years-long simulations of Meier (2007) showed also a pronounced inter-annual variability of winter convection. In March-April the re-stratification starts to form and the cold water is overlain by waters from the seasonal thermocline. As the time progresses after the maximum cooling, the cold water content of the CIL starts to decrease, which is seen in Fig. 8a as a decrease of its thickness. The refill and thickening of the CIL in winter and the decrease of its cold water content in summer repeats in an almost periodic way every year. These results demonstrate that the model replicates some of the known features and processes associated with the temporal evolution of thermohaline circulation in the Baltic Sea.

5.2 The Two-layer Exchange in the NBTZ

The widths of the straits in the NBTZ, i.e. the Great Belt, the Sound and the Little Belt, are 16-32 km, 4 km and 1 km respectively. The comparison of the straits widths with the internal

(baroclinic) Rossby radius of deformation (~5 km in the Kattegat) indicates that the Great Belt could be rotationally dominated. However all Baltic Sea straits are shallow and mostly friction-dominated. Furthermore the narrower ones are shaped by sills and contractions, which make the understanding of processes there difficult. In the following the simulations results are illustrated along three transects in the straits (Fig. 9a) for temperature and salinity sampled from the model outputs at 00:00, Jan. 17, 2012 and at 00:00, Feb. 18, 2012, for outflow and inflow conditions respectively. The bottom relief changes very differently along the three sections. The main sill for the Great Belt is the Darss Sill (383 km on the section). However it is not only this sill, which is practically outside the strait, but also the narrows that constrain the two-layer exchange. In the Little Belt the shallowest depths along the sections are close to the corresponding narrowest section. However in the Drodgen Sill is located at the southern entrance of the Sound whereas the narrowest section is located in the northern part of Sound between Helsingör and Helsingborg.

The overall conclusion from the cross-sections in Fig. 9 is that the straits decouple the water masses, which is better seen in the field of salinity under the outflow condition (Fig. 9 b, d, f). This is well pronounced in the Great Belt and the Sound by the tongue of Baltic Sea water propagating into the direction of Kattegat. In the Sound this tongue propagates with relatively low values north of the strait while the mixing along the wide and shallow Great Belt reduces substantially the salinity contrast. Therefore the salinity distribution is smoother in this strait and the isohalines rather vertical and the gravity flow-like pattern (high salinity at the bottom, not reaching the sea surface) is seen only beyond the Darss Sill. Unlike this strait, the Sound shows more classic estuarine patterns with far reaching intrusions in the Kattegat, and a gravity flow-like pattern just after the sill only during inflow situation (Fig. 9l). The situation in the Little Belt is rather different from the two wider straits. Here the water south of the sill is more stagnant, which enables higher salinity values south of the sill. However the salinity contrast peaks around the sill (Fig. 9b). Note that because the very narrow section of this strait the back-and-forth oscillations of salinity front in the Little Belt are not in phase with the ones of the main straits.

For the outflow period analyzed above the temperature in the Baltic Sea is higher or comparable with the one in Kattegat (Fig. 9c, e, g). The absolute maximum is below the sea surface, which again demonstrates that the strong salinity stratification is the main stabilizing factor. Another clear evidence of the dominant role of salinity is that the along-channel separation of temperature

follows the maximum extension of the Baltic plume. During the inflow phase the North Sea water is clearly identifiable by the warmer temperature; the temperature patterns (Fig. 9i, k, m) are very similar to the ones of salinity (Fig. 9 h, j, l).

5.3 The Water Mass Formation

5.3.1 The Cascading of Mixed North Sea Water into the Gotland Basin

The water mass formation in the Baltic Sea reflects the balance between the heat and water fluxes at the surface and in the straits. The latter is illustrated in Fig. 10a by the cascading of inflowing water from the straits area down into the Baltic proper (an animation of the gravity flow can be viewed at: http://ccrm.vims.edu/yinglong/TMP/anim_transect_TS_Darss_to_Gotland_new.zip). Physically this process has much in common with the major Baltic flow events. The situation shown in Fig. 10(a&b) happened in February, 2012, which is consistent with the overall occurrence of the major inflow events. However it is weaker and there is no sufficiently big volume of mixed North Sea water that reaches the deepest layers of the Gotland Deep. The analysis of the 500-day simulations indicates that the situation shown in Fig. 10 is repeated many times during the analyzed period but usually with a lesser intensity.

During most of the time the Bornholm Basin is filled with mixed North Sea water up to its sill depth. The halocline reveals seishes-like oscillations at the interface in these basins triggered by the inflowing water, which supports the concept of Jakobsen (1995). Under strong wind conditions these denser waters overshoot the sill and cascade into the next basin. Beyond the Stolpe Channel the inflowing bottom water undergoes strong mixing over the sloped bottom. Traces of this saltier and warmer water can be found as deep as 150-200m. In the deeper layers its penetration is better illustrated by temperature, which acts as a tracer in this salinity-dominated environment.

As far as the large-scale surface salinity patterns are concerned, the continuous decrease of salinity to the east and the thinner diluted layer to the west give a manifestation that the numerical model captures well the main characteristic of this sea being a huge estuary. The patterns of temporal variability illustrated in Fig. 10 demonstrate that the simulated water mass formation undergoes large transformations basin-wide.

5.3.2 The Ventilation of the upper layer

The surface ocean processes are presented by the temperature distribution in winter (Fig. 10b) and summer (Fig. 10d). The seasonal thermocline starts to form at the beginning of April as the warmer surface water overlies the cold surface water formed by previous winter cooling. The temperature continuously increases up to 22° C in August, but this surface layer never gets thicker than 20-40 m. Very close to its upper boundary, at about 40-50 m, is the core of CIL with temperatures lower than 3 °C. It extends towards the NBTZ where it flattens. In this area the CIL is subject to periodic back-and-forth oscillations caused by the inflowing-outflowing straits circulation. The CIL mixes with saltier water in the straits, and depending on the season propagates with the inflow as the warm bottom water in summer (Fig. 10d) or cold bottom water in winter (Fig. 10b). This mixed water mass cascades from one to the next "retention" basin on its way to the Baltic proper.

The formation of cold intermediate water along the analyzed cross-section starts first at the surface of the Gotland Deep and at the end of September the CIL outcrops. Local traces of anomalous (warmer or colder) waters entrapped below the CIL propagate down-slope as seen by the temperature pattern in the area between the Bornholm Basin and Gotland Deep (Fig. 10 b&d). Noteworthy is the sequence of cold and warm water intrusions at different depths in winter (Fig. 10b). Obviously the dominant stratification caused by salinity limits the depth of propagation of waters from the CIL. Below these cold intrusions, warm intrusions are propagating with the gravity currents at the bottom. The variety of intrusions of temperature compared to the patterns of salinity demonstrates again that temperature over most of the basin can be roughly considered as a passive tracer.

The refill of the Baltic Sea with cold water continues until the end of February. During this time part of the cold water is formed not only in the interior of the sea. In the shallower zone convection reaches the bottom and cold plumes propagate towards the deeper part of the basin. Because of the low salinities on the shelf their density is not high enough to reach deeper levels. Therefore these cold waters propagate in the direction of Gotland Deep as horizontal intrusions above the halocline contributing to additional cooling of the basin interior.

6. Conclusions

We have described here a new unstructured-grid model and its application to the North Sea and Baltic Sea, a region dominated by tides, inflows, shelf and baroclinic processes. The focus was on the NBTZ (North Sea - Baltic Sea Transition Zone) which is the most difficult area to simulate in the studied region because it requires very good quality of simulations of both barotropic and baroclinic processes. This zone is crucial for the processes developed on either side of straits (the Skagerrak and Norwegian Trench on one side, and the Baltic Sea on the other side). The specificity of the NBTZ in comparison to other similar zones is that its dynamics are controlled by multiple straits, the narrowest one being only 1km wide and the widest being about 16 km wide. With the setup of the presented model we resolved in a reasonable way these straits which ensured realism in the simulations of the exchange flows.

The model overcame some inconsistencies in earlier simulations that either covered only one sea (only Baltic or only North Sea) or used non-seamless one-way or two-way nesting techniques. The placement of the open-boundary conditions far from the straits made it possible that the model developed its own dynamics which appeared consistent with the tide gauges and temperature-salinity observations. Thus the presentation of the model validation appears one substantial part of the present research because this is a prerequisite for establishing some confidence in the interpretation of numerical simulations.

The statistical analysis of the simulated sea levels demonstrated that most of the analyzed North Sea stations tend to tightly follow the observations; the tidal variability is very well simulated. The dynamics of sea levels in the Baltic Sea are mostly driven by the evolution of weather systems although the responses greatly differ over different areas of the sea. Eigen oscillations also seem to have an important contribution to the Baltic Sea dynamics. The model captured all these important responses well.

The NBTZ presents an interesting case of reduction of the tidal range when the tides propagate through the straits. On the other hand, in this zone, the relative contribution from the weather systems (which is part of the barotropic forcing) increases because the straits amplify the sea-level contrasts between the Baltic Sea and North Sea. The reversal of the atmospherically driven barotropic gradient triggers the temporal change of surface-to-bottom salinity difference. This is clearly revealed in the variability of the vertical mixing and re-stratification, and is very well

validated by the similar variability seen in the observations. It is noteworthy that in this zone reversal of transports (inflow-outflow conditions) is well illustrated by the increased difference between the surface and bottom salinity values. With increasing distance from the straits other topographic features such as small basins (Arkona, Bornholm) start to play the role of reservoirs for denser water which under specific conditions propagates to the next (deeper) basin on its way to the Gotland Deep. In these areas the inflow resembles the gravity overflows. The individual inflow events were well captured by the model.

For the Baltic Sea modelling, simulating water mass formation is of particular importance because the distribution of water masses gives the major representation of the estuarine dynamics of this basin. The simulated refill and thickening of the CIL (cold intermediate layer) in winter and the propagation of cold water in summer demonstrated that the model successfully replicates the known features of the temporal evolution of thermohaline circulation in the Baltic Sea. Of particular interest is that the simulated SST demonstrated a good agreement with the OSTIA data. Furthermore, the evolution of CIL near the straits was also realistically simulated. This was illustrated by the realistic simulation of the mostly salinity-dominated vertical stratification and the cascading of inflowing water from the straits area down to the Baltic proper; the cascading inflow process is one important mechanism in maintaining the vertical conveyor belt (Döös et al., 2004).

Acknowledgements

We are grateful to the two anonymous reviewers for their constructive comments. S. Grashorn is funded by the initiative Earth Science Knowledge Platform (ESKP) operated by the Helmholtz Association. Y. Zhang was a HWK (Hanse-Wissenschaftskolleg) Fellow when he performed part of this work. The forcing data have been provided by the German Weather Service and NOAA. The river run-off data were provided by the Bundesamt für Seeschifffahrt und Hydrographie (BSH). Bathymetry data have been provided by BSH, DMI and Baltic Sea Hydrographic Commission, 2013 (Baltic Sea Bathymetry Database version 0.9.3). The authors are thankful to W. Koch for preparing the model forcing and B. Gardeike for assistance with the graphics. Simulations used in this paper were conducted on the following computational facilities: (1) Sciclone at the College of William and Mary which were provided with the assistance of the

National Science Foundation, the Virginia Port Authority, and Virginia's Commonwealth Technology Research Fund; (2) the Extreme Science and Engineering Discovery Environment (XSEDE; Grant TG-OCE130032), which is supported by National Science Foundation grant number OCI-1053575; (3) NASA's Pleiades; and (4) JUROPA at Jülich Supercomputing Centre (JSC), provided by the John von Neumann Institute for Computing (NIC).

Appendix 1. Choice of vertical grids

The important role of vertical grids in ocean models has long been recognized, and traditional choices (*Z*, terrain-following, or isopycnal coordinates) all suffer from certain shortcomings. Therefore we have recently proposed a new type of vertical grid that maximizes the flexibility in resolving processes of contrasting scales as found in the ocean, river and lake modeling (Zhang et al. 2015). Dubbed Localized Sigma Coordinates with Shaved Cell (LSC^2), it allows flexible placement of vertical grid nodes at each horizontal position while minimizing non-smoothness among neighboring nodes. The latter is ensured by the Vanishing Quasi Sigma (VQS) of Dukhovskoy et al. (2009). Moreover, the staircases found in VQS are eliminated with a novel and simple shaved cell technique that effectively shuts down the diapycnal mixing and in the same time, reduces the coordinate slope and thus the classic Pressure Gradient Errors (PGE; Haney 1991). Many tests have been conducted to demonstrate the superiority of the new LSC^2 grid (Zhang et al. 2015).

Fig. A1 further illustrates the superior results obtained from the LSC^2 grid. With the 31-level *S* grid, the physically stable stratification as found in the Baltic proper is gradually eroded over a few months due to a combination of PGE and diapycnal (numerical) mixing. Increasing the number of vertical levels to 51 only delayed the erosion by a few months, and adjusting the stretching parameters used in *S* did not significantly affect the results either (not shown). On the other hand, the new LSC^2 grid, despite having fewer number of levels on average, is able to maintain the stable stratification over multi-year simulations (also cf. Fig. 8b), which is crucial for Baltic Sea because the Major Inflow events only happen roughly over a ten-year scale.

Appendix 2. Validation of sea levels

We group the validation into 2 regions: NBTZ and Baltic Sea. The station coordinates can be seen in Table 1. Exemplary time series over a 14-day period and low-pass filtered signals are shown in Fig. A2. Some error statistics at 14 NBTZ stations are shown in Table 2, which can be compared with those in Fu et al. (2012). Tidal harmonics at North Sea stations are reported in Table 3. A mini-storm can be seen at the end of the 14-day period at most NBTZ stations, as a response to a weather system that dominated the region. No pronounced spring-neap cycle is found anywhere in the 2 regions, and while NBTZ stations exhibit some similarities among each other, the Baltic stations show greater disparity suggesting localized responses. For example, many Baltic stations did not witness the set-down near Day 148, and some show distinctive period of oscillation of a few days (#26, 30, 39, 73). Overall, the model captured both system-wide and localized responses pretty well.

Table 1. NBTZ and Baltic stations location

Station	Lon	Lat	Station	Lon	Lat	Station	Lon	Lat	Station	Lon	Lat
Aarhus	10.2167	56.15	Hornbaek	12.4667	56.1	Marviken	16.8371	58.5537	Smogen	11.2178	58.3537
Althagen	12.4194	54.3769	Juelsminde	10.0167	55.7167	Neustadt	10.8128	54.0967	Soru	22.5229	58.6938
Bagenkop	10.6778	54.7528	Kalix	23.0962	65.697	NordreRose	12.6867	55.6361	Spikarna	17.5312	62.3632
Ballen	10.6444	55.8167	Kalkgrund	9.8881	54.8247	Olands NorraUdde	17.0971	57.3662	StPetersburg	30.2667	59.9333
Barhoeft	13.0328	54.4397	Kappeln	9.9381	54.6644	Oskarshamn	16.4779	57.2749	Stenungsund	11.8325	58.0933
Barseback	12.9034	55.7565	Kaskinen	21.2167	62.3333	Paldiski	24.0796	59.3349	Stockholm	18.0818	59.3243
Daugavgriva	24.0167	57.05	Kemi	24.5167	65.6667	Pietarsaari	22.7	63.7	Stralsund	13.0986	54.3153
Degerby	20.3833	60.0333	KielHoltenau	10.1569	54.3722	Ratan	20.895	63.9861	Tallinn	24.7637	59.4444
Drogden	12.7117	55.5358	KielLT	10.2733	54.4997	Ringhals	12.1126	57.2498	Tejn	14.8333	55.25
Eckernfoerde	9.8361	54.4747	Klagshamn	12.8936	55.5223	Rodby	11.35	54.65	TimmendorfPoel	11.3756	53.9919
Flensburg	9.4331	54.795	Klaipeda	21.0833	55.7333	Rodvig	12.3728	55.2542	Travemuende	10.8722	53.9581
Forsmark	18.2109	60.4085	Kobenhavn	12.6	55.7	Rohukula	23.4248	58.9049	Triigi	22.7173	58.5914
Fredericia	9.75	55.5667	Kolka	22.5833	57.7333	Rostock	12.155	54.0831	Ueckermuende	14.0664	53.7503
Frederikshavn	10.5667	57.4333	Korsor	11.1333	55.3333	Sassnitz	13.6431	54.5108	Viken	12.5793	56.1421
Furuogrund	21.2306	64.9157	Koserow	14.0008	54.0603	Schleimuende	10.0367	54.6733	Virtsu	23.5081	58.5761
Fynshav	9.9833	55	Kronstadt	29.75	59.9667	Schleswig	9.5692	54.5114	Visby	18.2845	57.6393
Gedser	11.9333	54.5667	Kuivastu	23.3935	58.5742	Sillamae	27.7401	59.4227	Warnemuende	12.1033	54.1697
Goteborg Torshamnen	11.7907	57.6846	Kungsholmsfort	15.5893	56.1052	Simrishamn	14.3577	55.5576	Wismar	11.4581	53.8989
Greifswald	13.4461	54.0928	Kungsvik	11.1274	58.9966	SjaellandsOdde	11.3722	55.975	WittowerFahre	13.245	54.5575
Grena	10.9306	56.4111	LandsortNorra	17.8589	58.7688	Skagen	10.5858	57.7194	Wolgast	13.7703	54.0417
Heiligenhafen	11.0056	54.3731	Langballigau	9.6542	54.8233	Skagsudde	19.0124	63.1905			
Helsinki	24.9667	60.15	Lehtma	22.6969	59.069	Skanor	12.8296	55.4168			

Heltermaa	23.0466	58.8664	Luebeck	10.7031	53.8931	Slipshavn	10.8333	55.2833			

629

630 Table 2. Elevation error statistics at the 14 NBTZ stations used in Fu et al. (2012).

	Correlation coefficient	Unbiased RMSE (m)	Bias (m)
Aarhus	0.875	0.073	0.045
Frederikshavn	0.919	0.063	0.136
Slipshavn	0.800	0.067	0.046
Korsor	0.806	0.057	-0.003
Hornbæk	0.983	0.046	-0.030
Rodby	0.893	0.043	0.077
Gedser	0.908	0.043	0.017
Tejn	0.915	0.043	0.157
Kalix	0.966	0.049	0.329
Klagshamn	0.878	0.051	0.108
Kungsholmsfort	0.891	0.063	0.149
Kungsvik	0.925	0.030	0.112
Ratan	0.958	0.061	0.307
Visby	0.873	0.060	0.201

631

632 Table 3. Comparison of **M2** (which accounts for over 80% of the total tidal energy) amplitudes
633 and phases at North Sea stations.

Station name	Amp_Obs (m)	Amp_Mod (m)	Pha_Obs (degr)	Pha_Mod (degr)
Aberdeen	1.24	1.09	21.75	21.39
Bournemouth	0.41	0.52	271.82	273.00
Cromer	1.56	1.29	187.23	193.60
Dover	2.24	2.08	330.17	324.30
Harwich	1.32	1.32	323.84	320.15
Immingham	2.23	1.96	160.63	165.80
Jersey	3.29	3.30	176.57	175.29
Lowestoft	0.68	0.62	259.15	262.13
Newhaven	2.21	2.12	319.04	303.65
North Shields	1.60	1.34	84.66	88.08
Wick	1.01	0.91	320.81	326.75
Borkum	1.11	1.16	273.67	263.63
Helgoland	1.11	1.17	308.42	296.86
Hirtshals	0.15	0.20	107.10	113.21

634

635 **Figure captions**

636 **Fig. 1**. North Sea and Baltic Sea topography. The color scheme was chosen to better illustrate the
637 bottom relief in the deepest parts of the two basins. The positions of the following stations used
638 in model validation are also shown: (1) Jersey, (2) FINO-1, (3) Helgoland, (4) Frederikshavn, (5)
639 Fehmarn Belt, (6) Drogden, (7) Arkona Basin, (8) Tejn, (10) Kronstadt and (11) Kemi. Analyses

of numerical simulations are presented further in the paper at location (9) and along the transect line starting in the western Arkona Basin and ending in the northern Gotland Deep (grey line).

Fig. 2. Model grid size (a), and illustration of the fine grid resolution in the Great Belt (b), which is a zoom-in view of the rectangular box in (a).

Fig. 3. Modelled and observed sea level in Jersey (a), Helgoland (b), Tejn (c), Kronstadt (d), Kemi (e), Frederikshavn (f), Drogden (g). Red: observations; green: model (hourly time series).

Fig. 4.Taylor diagram of the modelled sea levels. The distance from the origin measures the RMSE of model results, scaled against standard deviation of the data. The correlation coefficients are shown on the full sector line (increasing from "North" to "East"). The purple star is the 'truth'. Black circles are the North Sea stations, red ones the NBTZ and the blue ones the Baltic Sea stations. The average correlation is 0.8837, and average scaled RMSE is 0.19. The stations used for this validation are shown in Table 1.

Fig. 5. Time series comparison between the simulated (blue lines) and observed (red dotted lines) near-surface and near-bottom salinities at the station Fehmarn Belt (see Fig. 1 for its positions). The near-surface values are lower than the near-bottom ones.

Fig. 6. Time versus depth diagrams of temperature (a, b) and salinity (c, d) in Arkona Basin. (a) and (c) are from observation and (b) and (d) are from model.

Fig. 7. The RMSE (a) and mean bias (b) of SST between model and OSTIA data. The blank areas in Baltic Sea are due to missing data at some time instances, and the local extrema in the northern part of North Sea is due to OSTIA issue. The black isoline in (b) is the boundary between positive and negative biases.

Fig. 8. Time versus depth diagrams of temperature (a) and salinity (b) at the Gotland Basin (see location 9 in Fig. 1). The isolines in (a) represent 3, 3.5, 4, 4.5^{o}C.

Fig. 9. Vertical cross-sections of salinity (left panels) and temperature (right panels) along 3 transects in Little Belt (b, c, h, i), Great Belt (d, e, j, k) and Sound (f, g, l, m). (b-g) represent the outflow conditions at 00:00, Jan. 17, 2012, and (h-m) represent the inflow conditions at 00:00, Feb. 18, 2012. The black dashed line shows where the transect coming from Little Belt joins the transect coming from Great Belt. In all plots, x=0 corresponds to the starting location in the north. The locations of the three transects are shown in (a).

Fig. 10. Water masses in the Baltic Sea along the section shown in Fig. 1. (a) is salinity on Feb. 29, 2012, (b) is temperature on Feb. 29, 2012; (c) is salinity on Aug. 02, 2012, and (d) is temperature on Aug. 02, 2012.

Fig. A1 Comparison of salinity profile at Gotland Deep (see Fig. 1 for location), from Nov. 1, 2013 to Feb. 1, 2014, using (a) 31 S layers, and (b) LSC^2 grid. See Section 2.3 for more details of the two types of vertical grids used.

Fig. A2 Comparison of elevations at (a) NBTZ and (b) Baltic Sea stations. The station locations are shown in Table 1. The red lines are observation, and green lines are model results. The x-axis is time in days from July 1, 2011. (c) and (d) show the low-pass filtered signals (with 30-hour cut-off) for (a) and (b) over a longer period.

References

Azevedo, A., Oliveira, A., Fortunato, A.B., Zhang, Y. and Baptista, A.M. (2014) A cross-scale numerical modeling system for management support of oil spill accidents, *Marine Pollution Bulletin*, 80, 132-147.

Baptista, A.M., Zhang, Y., Chawla, A., Zulauf, M.A., Seaton, C., Myers, E.P., Kindle, J., Wilkin, M., Burla, M. and Turner, P.J. 2005 A cross-scale model for 3D baroclinic circulation in estuary-plume-shelf systems: II. Application to the Columbia River. *Continental Shelf Research*, 25, 935-972.

Bell, M.J., Forbes, R.M., and Hines, A. (2000). Assessment of the FOAM global data assimilation system for real-time operational ocean forecasting. *J. Mar. Syst*., 25 (1), 1-22.

Bendtsen, J., K. E. Gustafsson, J. Söderkvist, J. L.S. Hansen, (2009) Ventilation of bottom water in the North Sea–Baltic Sea transition zone, Journal of Marine Systems, Volume 75, Issues 1–2, Pages 138-149,

Bertin, X., Li, K., Roland, A., Zhang, Y., Breilh, J.F. and Chaumillon, E. (2014) A modeling-based analysis of the flooding associated with Xynthia, central Bay of Biscay, *Ocean Eng*, 94,80-89.

Burchard, H , Lass, U., Mohrholz, V., Umlauf, L., Sellschopp J., Fiekas, V., Bolding, K., and Arneborg, L. (2005) Dynamics of medium-intensity dense water plumes in the Arkona Sea, Western Baltic Sea, *Ocean Dynamics*, 55: 391-402.

Burchard, H., Janssen, F., Bolding, K., Umlauf, L., Rennau, H. (2009), *Cont Shelf Res*., 29:205-220.

Danilov, S. (2013) Ocean modeling on unstructured meshes, *Ocean Mod.*, 69, 195-210. doi: 10.1016/j.ocemod.2013.05.005

Donlon, C.J., Casey, K.S., Robinson, I.S., Gentemann, C.L., Reynolds, R.W., Barton, I., Arino, O., Stark, J., Rayner, N., Le Borgne, P., Poulter, D., Vazquez-Cuervo, Armstrong, E., Beggs, H., Llewellyn-Jones, D., Minnett, P.J., Merchant, C.J., and Evans, R. (2009) The GODAE High Resolution Sea Surface Temperature Pilot Project, *Oceanogr*., 22 (3), 34-45.

Döös, K., H. E. M. Meier, and R. Döscher (*2004*) The Baltic Haline Conveyor Belt or The Overturning Circulation and Mixing in the Baltic. AMBIO: A Journal of the Human Environment: June 2004, Vol. 33, No. 4, pp. 261-266.

Dukhovskoy, D.S., Morey, S.L., O'Brien, J.J., Martin, P.J., and Cooper, C. (2009) Application of a vanishing quasi-sigma vertical coordinate for simulation of high-speed deep currents over the Sigsbee Escarpment in the Gulf of Mexico, *Ocean Mod*., 28, 250–265.

Feistel, R., Nausch, G., Matthäus, W., and Hagen, E. (2003a) Temporal and spatial evolution of the Baltic deep water renewal in spring 2003, *Oceanologia*, 45(4), 623–642.

Feistel, R., Nausch, G., Mohrholz, V., Łysiak-Pastuszak, E., Seifert, T., Matthäus, W., Krüger, S., Sehested-Hansen, I. (2003b) Warm waters of summer 2002 in the deep Baltic Proper. Oceanologia, 45 (4), 571–592

Feistel, R., Nausch, G., and Hagen, E. (2006) Unusual inflow activity in 2002–2003 and varying deep-water properties, *Oceanologia*, 48(S), 21–35.

Fu, W., Høyer, J.L., and She, J. (2011) Assessment of the three dimensional temperature and salinity observational networks in the Baltic Sea and North Sea, *Ocean Sci*., 7, 75- 90, doi:10.5194/os-7-75-2011.

Fu, W., She, J., and Dobrynin, M. (2012) A 20-year reanalysis experiment in the Baltic Sea using three-dimensional variational (3DVAR) method, *Ocean Sci*., 8, 827-844, doi:10.5194/os-8-827-2012, 2012.

Funkquist, L. and Kleine, E. (2007) An introduction to HIROMB, an operational baroclinic model for the Baltic Sea. Technical report No 37, 2007. SMHI. Norrköping, 47 pp.

Haney, R.L. (1991) On the pressure gradient force over steep topography in sigma coordinate ocean models, *J. Phys. Oceanogr*., 21, 610–619.

Jakobsen, F. (1995) The major inflow to the Baltic Sea during January 1993, *J Mar Syst*, 6:227-240.

Janssen, F., Schrum, C., and Backhaus, J. (1999) A climatological data set of temperature and salinity for the Baltic Sea and the North Sea, *Deut. Hydrogr. Z., supp*., 9, 5–245.

735 Kliem, N., Nielsen, J.W. and Huess, V. (2006) Evaluation of a shallow water unstructured mesh
736 model for the North Sea - Baltic Sea. *Ocean Mod.*, 15(1-2), 124-136,
737 doi:10.1016/j.ocemod.2006.06.003

738 Lehmann, A., Lorenz, B., and Jacob, D. (2004) Modelling the exceptional Baltic Sea inflow
739 events in 2002-2003, *Geopghys. Res. Lett*., 31 L21308, doi: 10.1029/2004GL020830.

740 Leppäranta, M. and Myrberg. K. (2009) Physical oceanography of the Baltic Sea. Springer,
741 Berlin, 378pp.

742 Liu, Y., H. E. M. Meier, and L. Axell (2013), Reanalyzing temperature and salinity on decadal
743 time scales using the ensemble optimal interpolation data assimilation method and a 3-D
744 ocean circulation model of the Baltic Sea, *J. Geophys. Res.-Oceans*, 118, 5536–5554,
745 doi:10.1002/jgrc.20384

746 Meier, H.E.M. (2001) On the parameterization of mixing in three-dimensional Baltic Sea
747 models, *J Geophys Res-Oceans*, 106:30,997–31,016

748 Meier, H.E.M. (2005) Modeling the age of Baltic Seawater masses: Quantification and steady
749 state sensitivity experiments, *J Geophys Res*, 110, C02006, doi:10.1029/2004JC002607

750 Meier, H.E.M. (2007) Modeling the pathways and ages of inflowing salt- and freshwater in the
751 Baltic Sea, *Estuarine Coastal Shelf Sci.*, 74 (4), 610–627.

752 Meier, H.E.M. and Kauker, F. (2003) Sensitivity of the Baltic Sea salinity to the freshwater
753 supply, *Clim Res*, 24: 231–242.

754 Omstedt, A., Elken, J., Lehmann, A., Leppäranta, M., Meier, H.E.M., Myrberg, K., and
755 Rutgersson, A. (2014) Progress in physical oceanography of the Baltic Sea during the 2003–
756 2014 period. *Progress in oceanography*, 128, 139-171.

757 Paulson, C.A. and Simpson, J.J. (1977) Irradiance Measurements in the Upper Ocean, *J. Phys.*
758 *Oceanogr*., 7, 952-956.

759 Pinto, L., Fortunato, A.B., Zhang, Y., Oliveira, A. and Sancho, F.E.P. (2012) Development and
760 validation of a three-dimensional morphodynamic modelling system, *Ocean Mod.*, 57-58,
761 1-14.

762 Rodrigues, M., Oliveira, A., Queiroga, H., Fortunato, A.B. and Zhang, Y.J. (2009) Three-
763 Dimensional Modeling of the Lower Trophic Levels in the Ria de Aveiro (Portugal),
764 *Ecological Modelling*, 220, 1274-1290.

765 Sannino G., Pratt, L. and Carillo, A. (2009) Hydraulic Criticality of the Exchange Flow through
766 the Strait of Gibraltar, *J. Physical Oceanography*, 39(11), 2779-2799.DOI:
767 10.1175/2009JPO4075.1

768 She, J., Berg, P. and Berg, J. (2007) Bathymetry impacts on water exchange modelling through
769 the Danish Straits. *J. Marine Systems*, 65, 450–459.

770 Schmidt, M., Fennel, W., Neumann, T. and Seifert, T. (2008) Description of the Baltic Sea with
771 numerical models. In: State and evolution of the Baltic Sea, 1952 – 2005. Ed. by R. Feistel,
772 G. Nausch and N. Wasmund. Hoboken: Wiley-Interscience: 583-624pp.

773 Stanev, E.V., Staneva. J.V. and Roussenov. V.M. (1997) On the Black Sea water mass
774 formation. Model sensitivity study to atmospheric forcing and parameterization of physical
775 processes. *J Mar Syst*., 13:245–272.

776 Stigebrandt, A. (1987) A model for the vertical circulation of the Baltic deep water, *J. Phys.*
777 *Oceanogr.*, 17, 1772–1785.

778 Stanev, E.V. and Lu, X. (2013) European semi-enclosed seas: basic physical processes and their
779 numerical modelling. In T. Soomere and E. Quak, Preventive methods for coastal
780 protection, 131-179, Springer, Switzerland, DOI: 10.1007/978-3-319-859 00440-2_5.

781 Stanev, E.V., Lu, X. Grashorn, S. (2015) Physical processes in the transition zone between North
782 Sea and Baltic Sea. Numerical simulations and observations, *Ocean Mod (accepted)*.

783 Umlauf, L. and Burchard, H. (2003) A generic length-scale equation for geophysical turbulence
784 models. *J. Mar. Res*., 6, 235-265.

785 Wang, H.V., Wang, Z., Loftis, J.D., Teng, Y.C. (2013) Hydrodynamic and water quality
786 modeling and TMDL development for Maryland's coastal Bays system, Final report
787 submitted to Maryland Department of the Environment, TMDL Technical Development
788 Program.

789 Willmott, C.J. (1981) On the validation of models, *Phys. Geogr*., 2,184–194.

790 Zeng, X., Zhao, M. and Dickinson, R.E. (1998) Intercomparison of bulk aerodynamic algorithms
791 for the computation of sea surface fluxes using TOGA COARE and TAO data. *J. Clim*.,
792 11, 2628-2644.

793 Zhang, Y. and Baptista, A.M. (2008) SELFE: A semi-implicit Eulerian-Lagrangian finite-
794 element model for cross-scale ocean circulation, *Ocean Mod.*, 21(3-4), 71-96.

795 Zhang, Y., Witter, R.W. and Priest, G.P. (2011) Tsunami-Tide Interaction in 1964 Prince
796 William Sound Tsunami, *Ocean Mod.*, 40, 246-259.

797 Zhang, Y., Ateljevich, E., Yu, H-S., Wu, C-H., and Yu, J.C.S. (2015) A new vertical coordinate
798 system for a 3D unstructured-grid model, *Ocean Mod.*, 85, 16-31.

799 Zhang, Y., Ye, F., Stanev, E.V. and Grashorn, S. (submitted) Seamless cross-scale modelling
800 with SCHISM, *Ocean Mod.*

801 Zhuang, S.Y., Fu, W.W., and She, J. (2011) A pre-operational three Dimensional variational data
802 assimilation system in the North/Baltic Sea, *Ocean Sci*., 7, 771–781, doi:10.5194/os-7-
803 771-2011.

Figure1

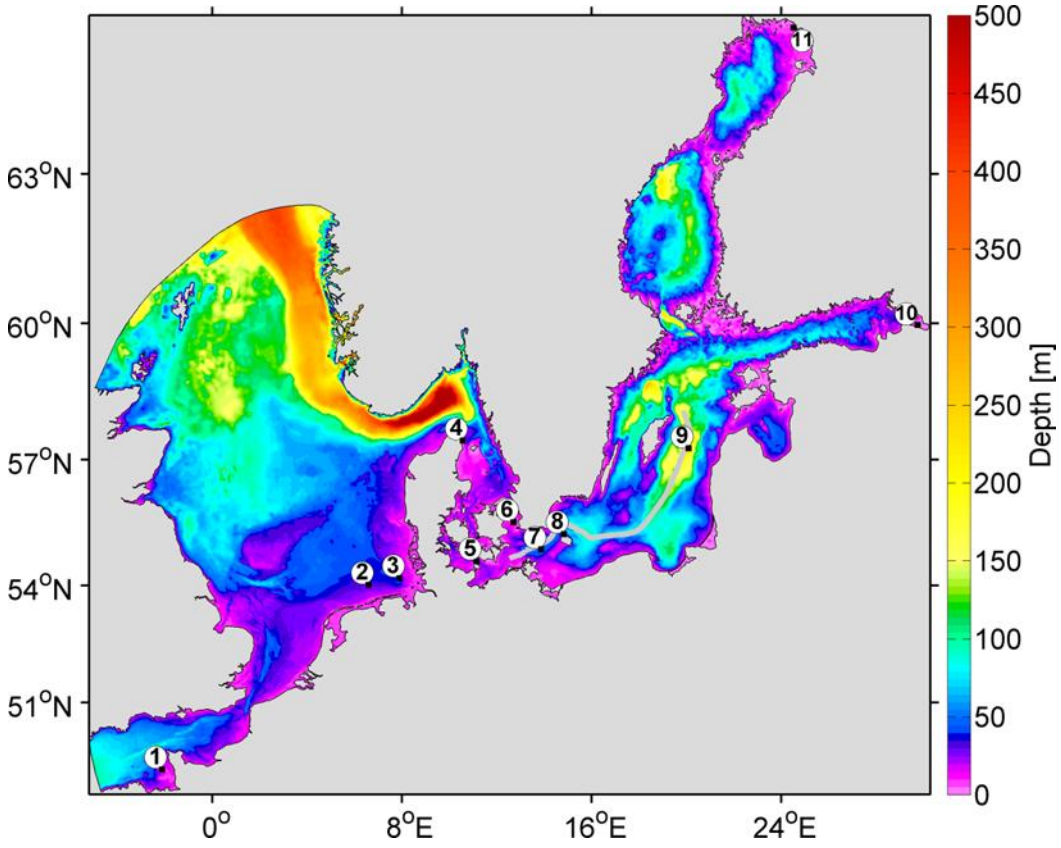

Fig. 1

Figure2

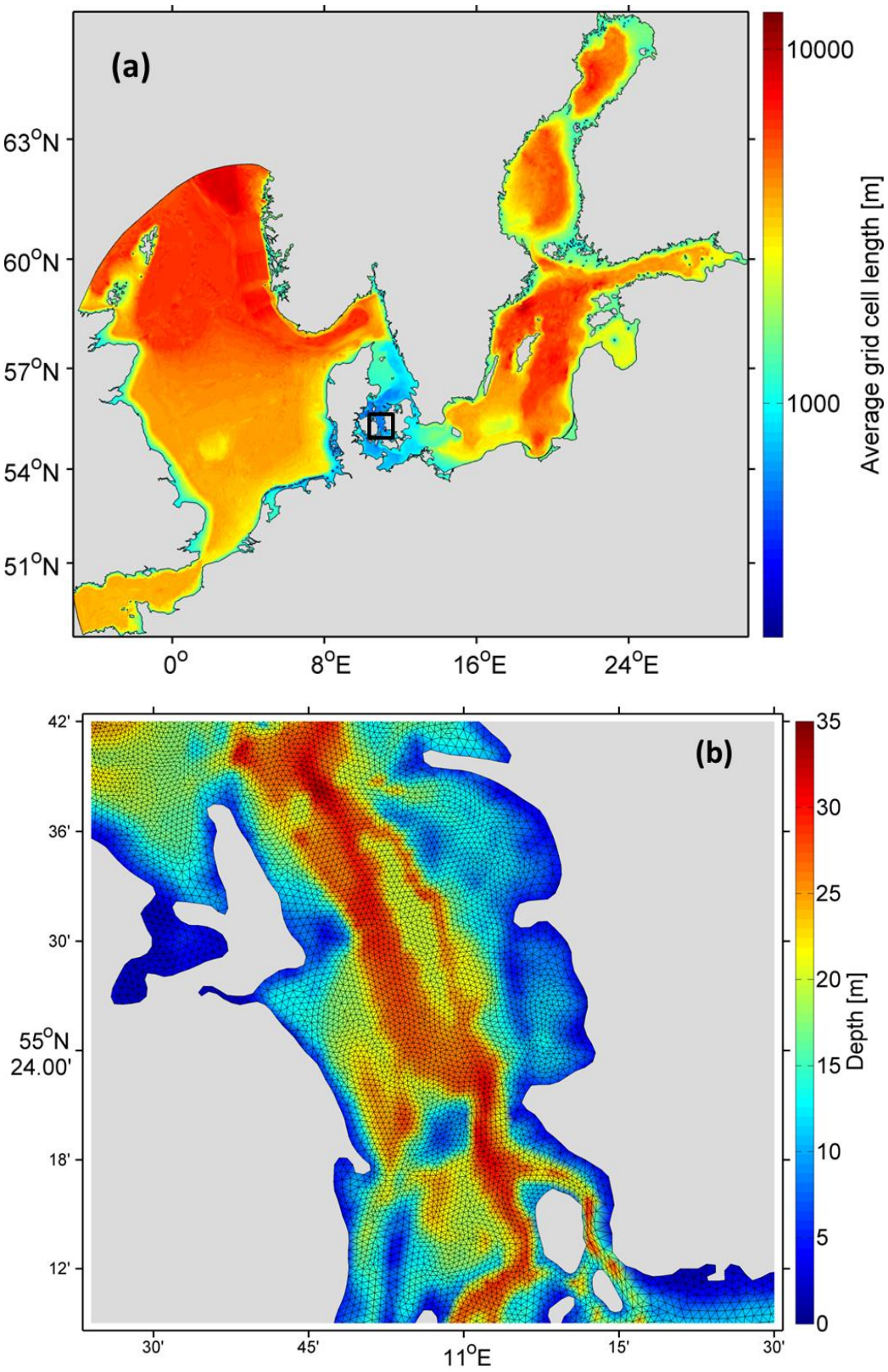

Fig. 2

Figure3

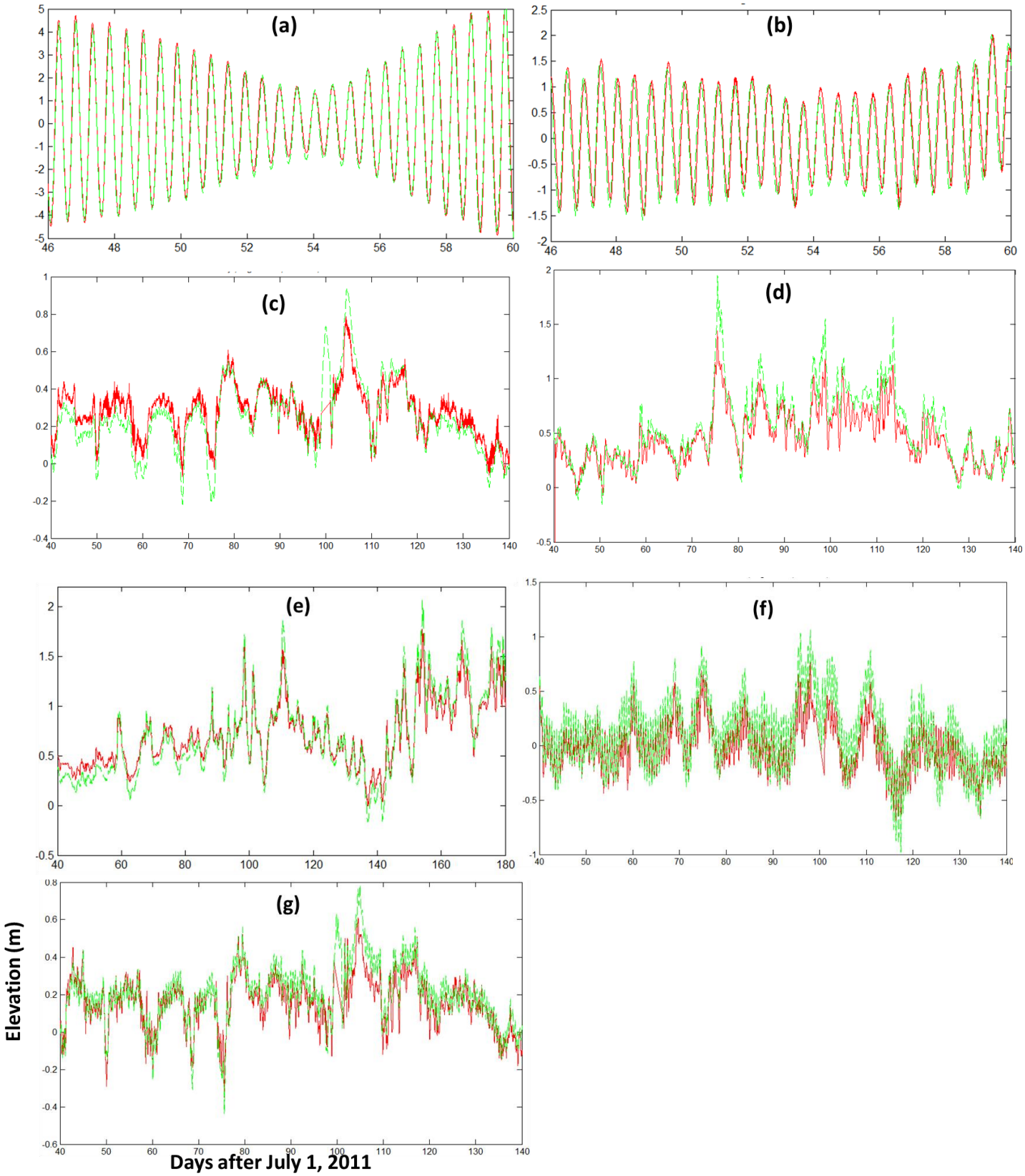

Fig. 3

Figure4

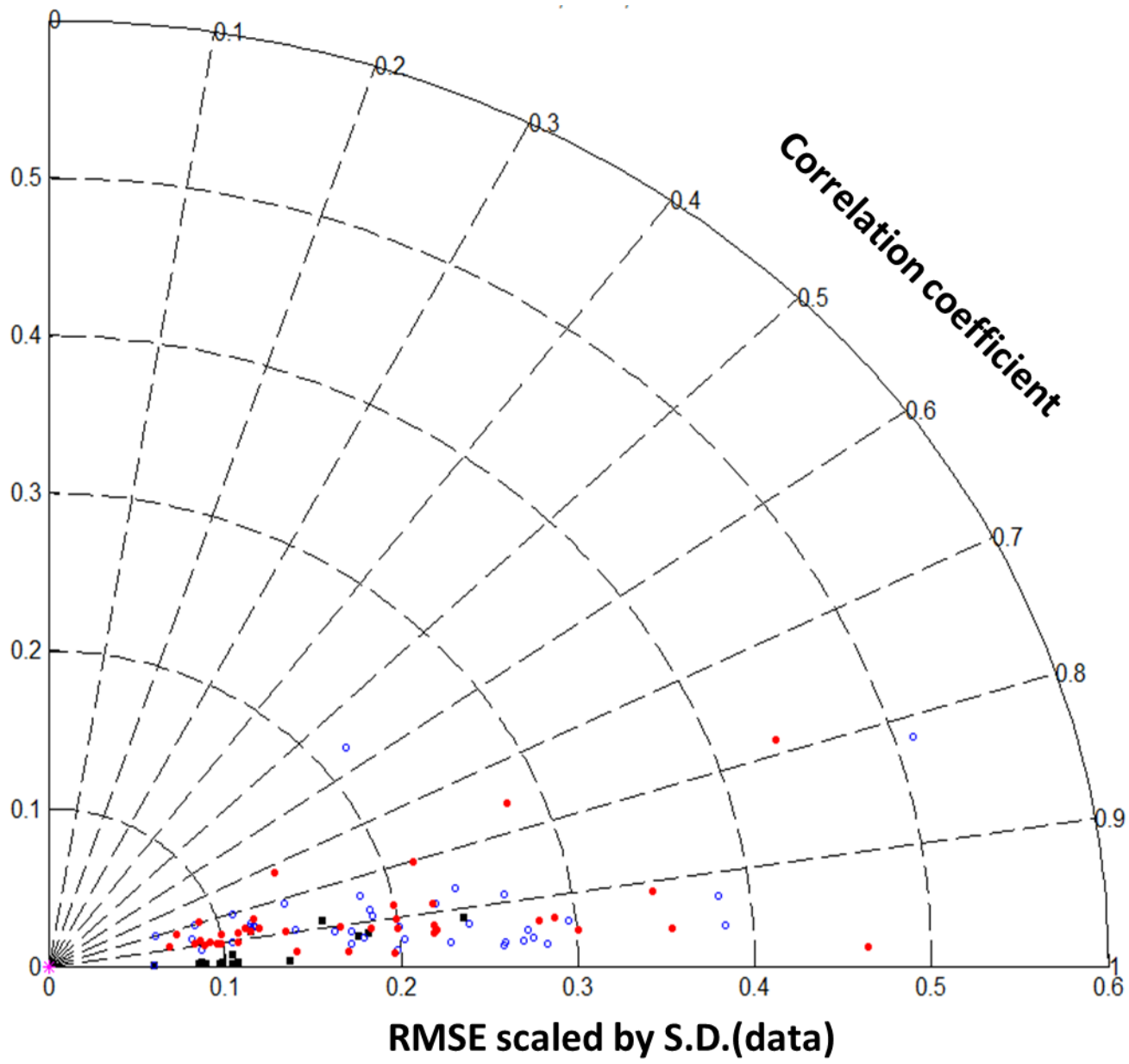

Fig. 4

Figure5

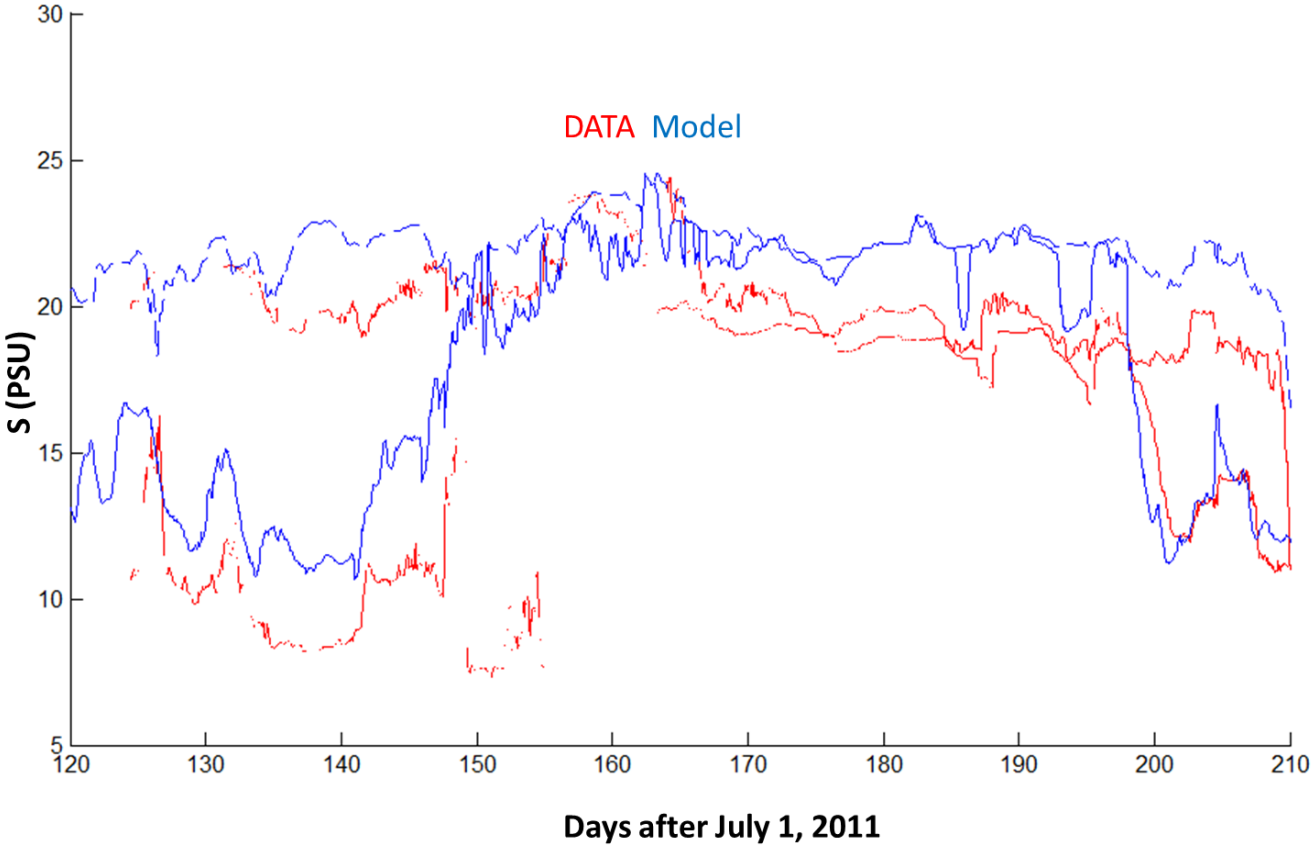

Fig. 5

Figure6

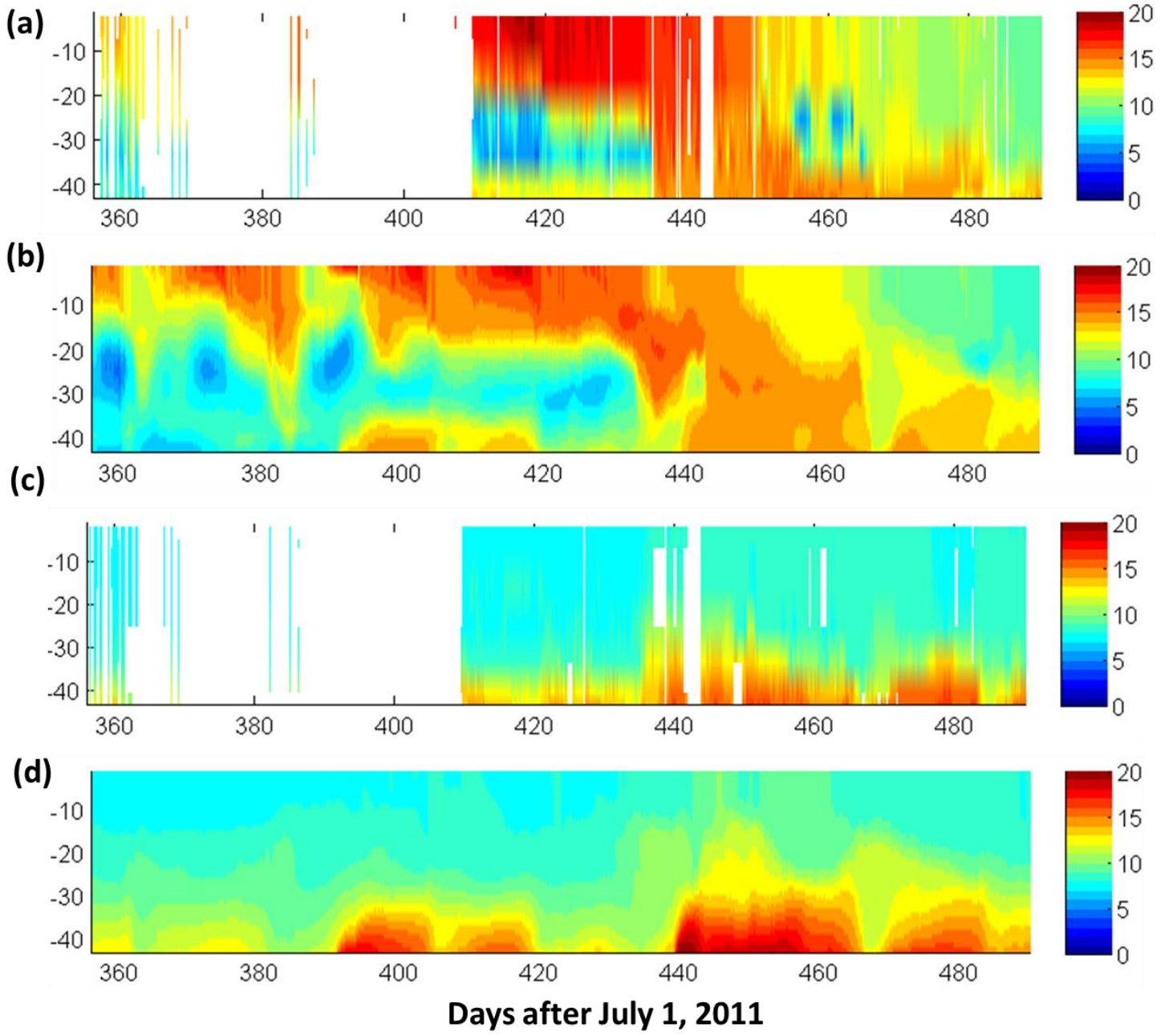

Fig. 6

Figure7

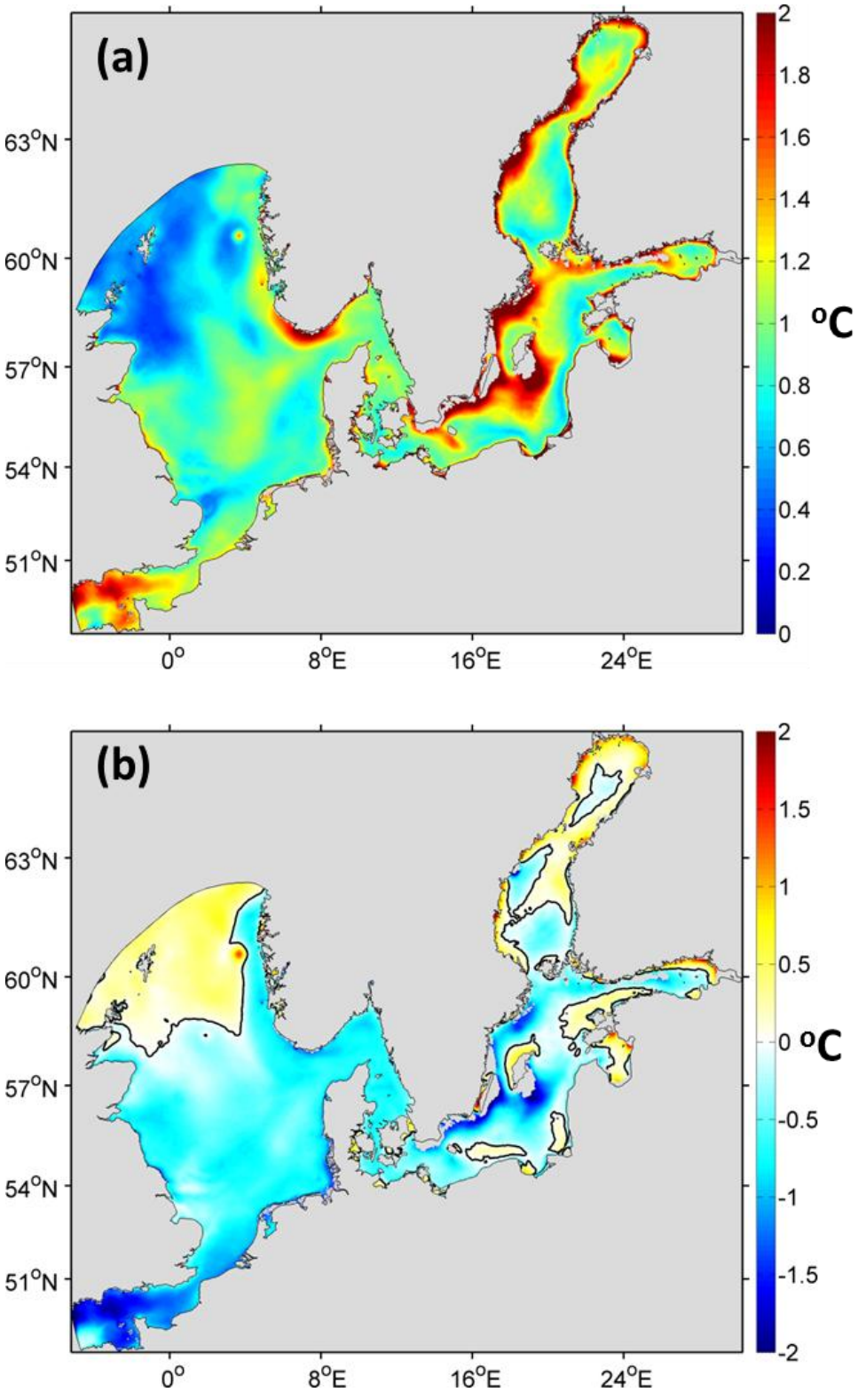

Fig. 7

Figure8

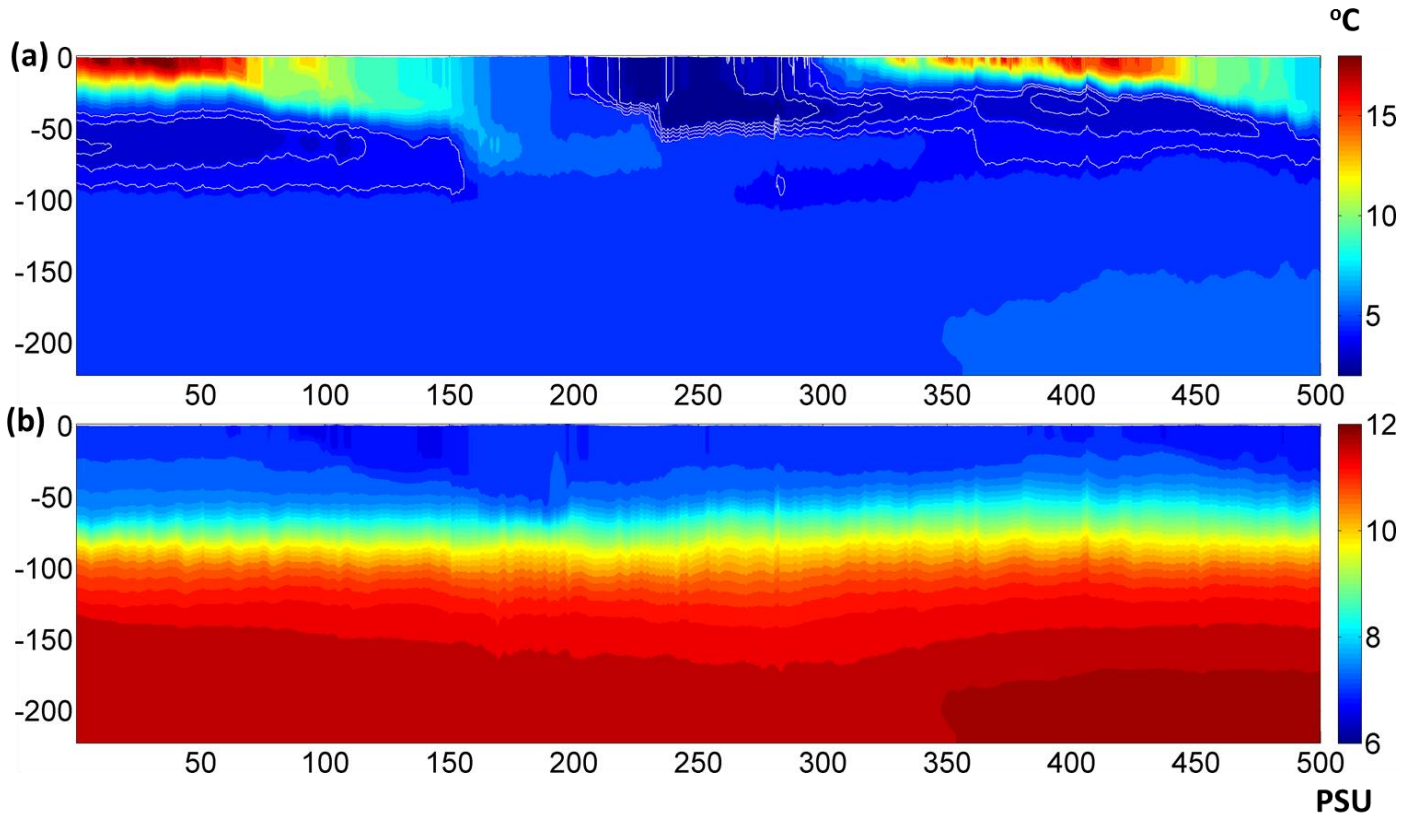

Fig. 8

Figure9

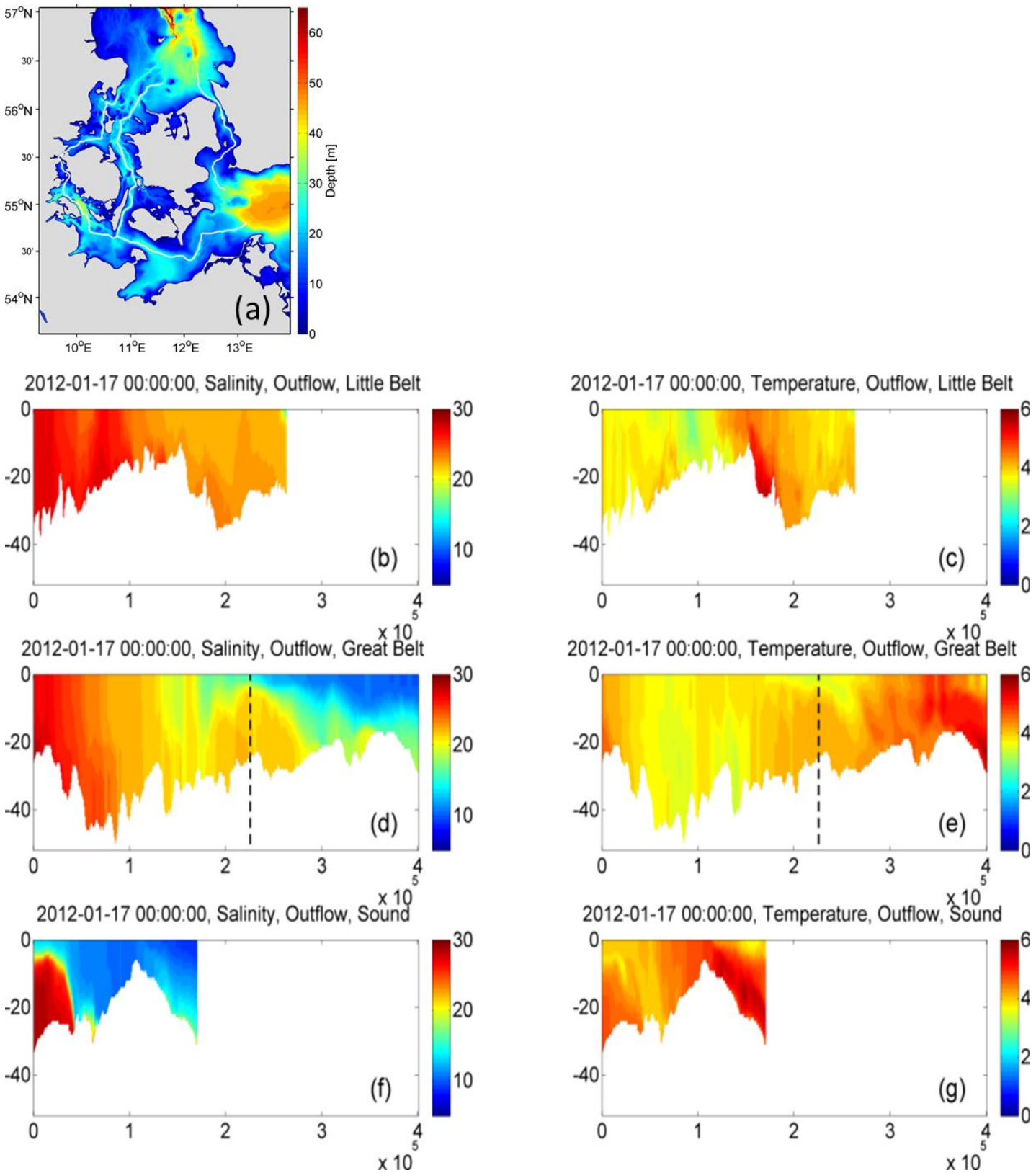

Fig. 9

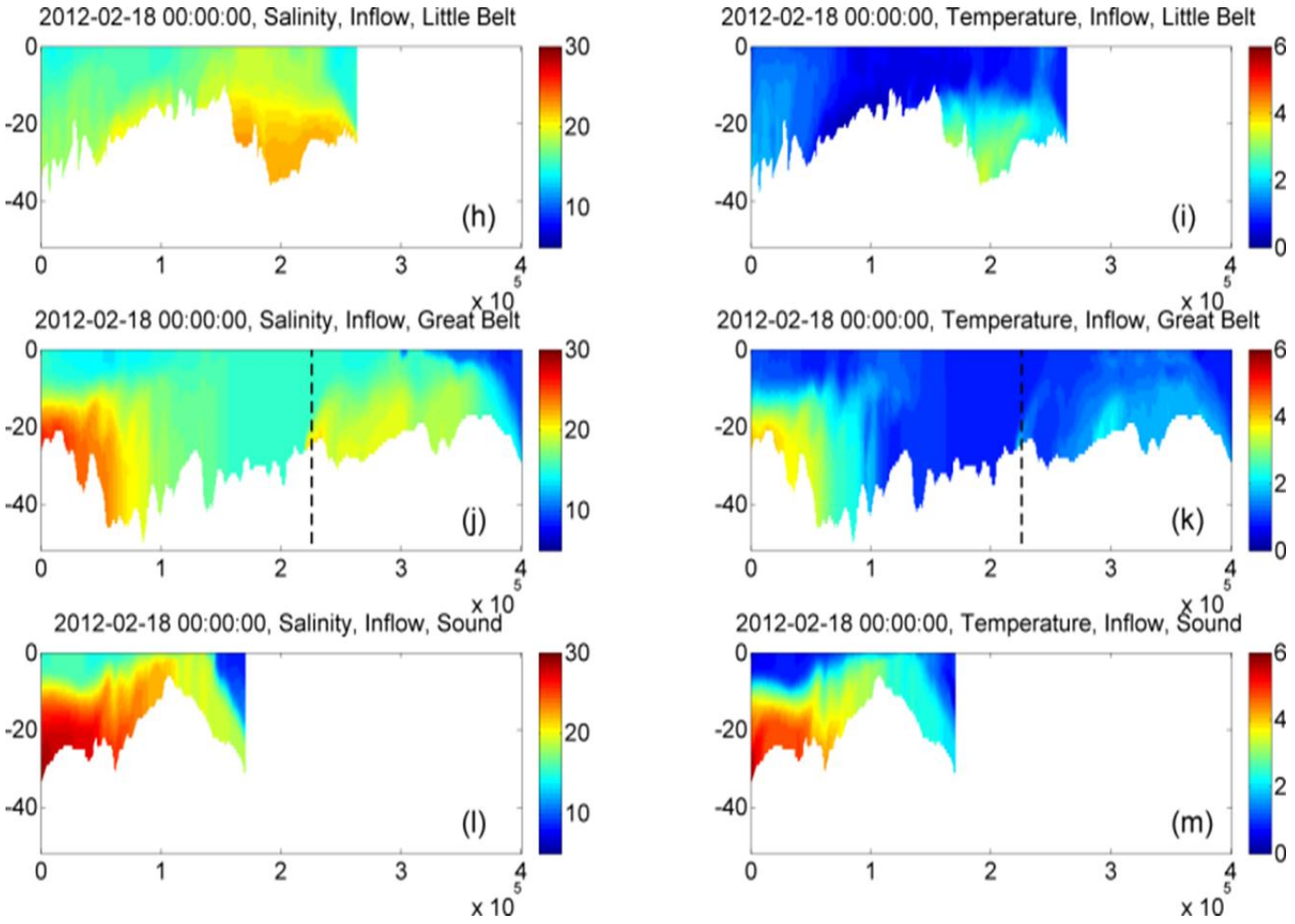
2012-02-18 00:00:00, Salinity, Inflow, Little Belt
2012-02-18 00:00:00, Temperature, Inflow, Little Belt
2012-02-18 00:00:00, Salinity, Inflow, Great Belt
2012-02-18 00:00:00, Temperature, Inflow, Great Belt
2012-02-18 00:00:00, Salinity, Inflow, Sound
2012-02-18 00:00:00, Temperature, Inflow, Sound
(h)
(i)
(j)
(k)
(l)
(m)
x 10^5

Fig. 9

Figure10

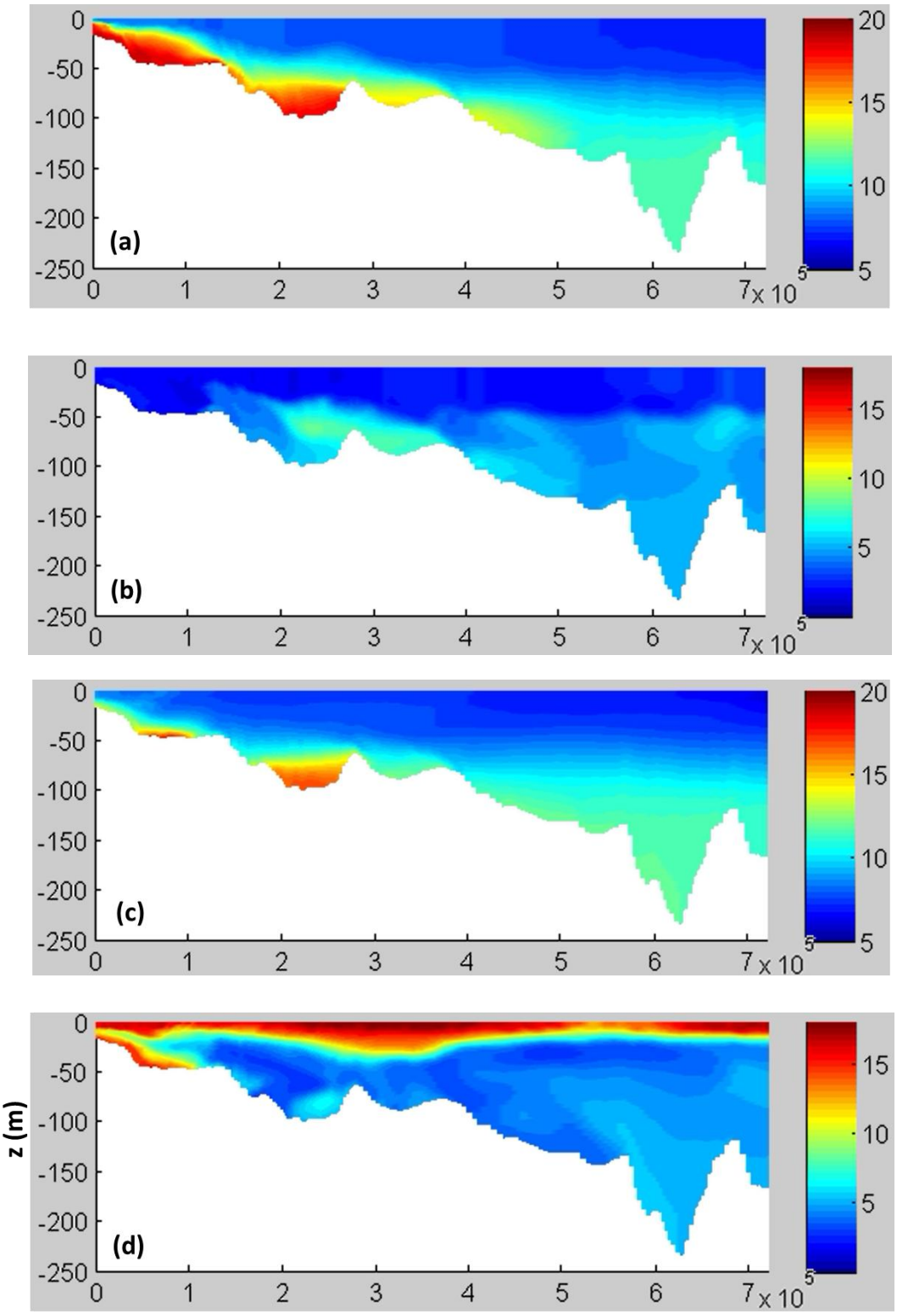

Fig. 10

FigureA1

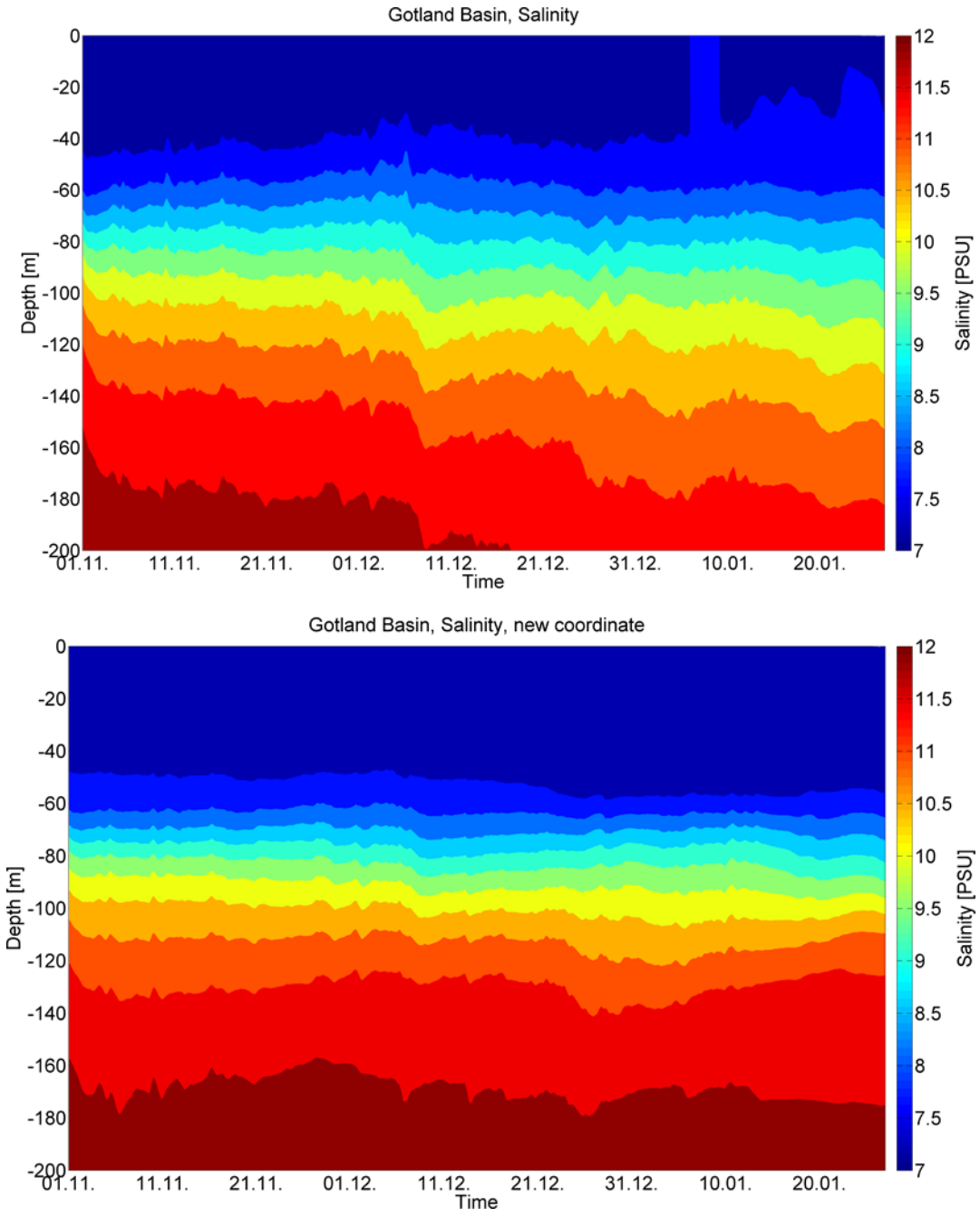

Fig. A1

FigureA2

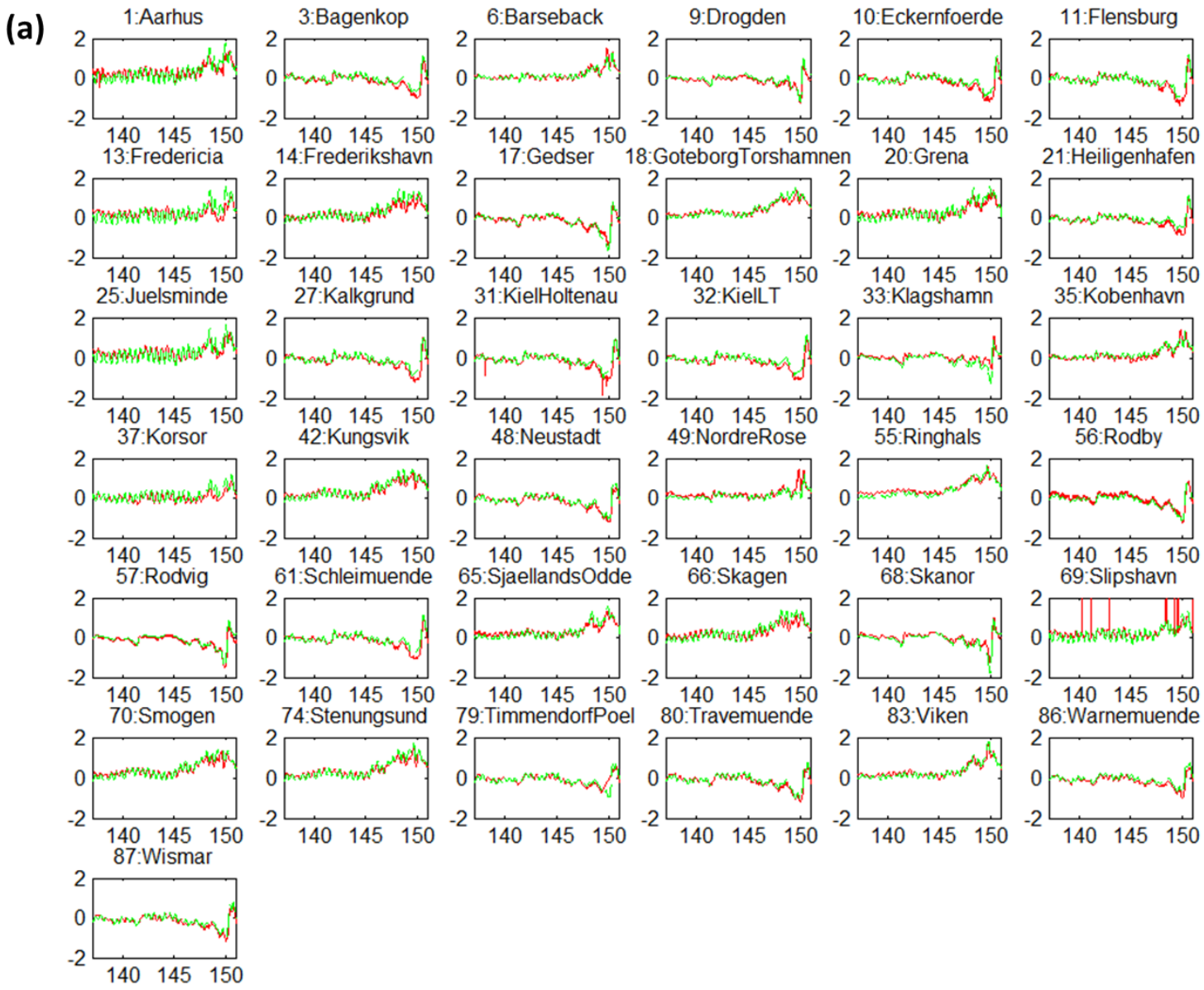

Fig. A2

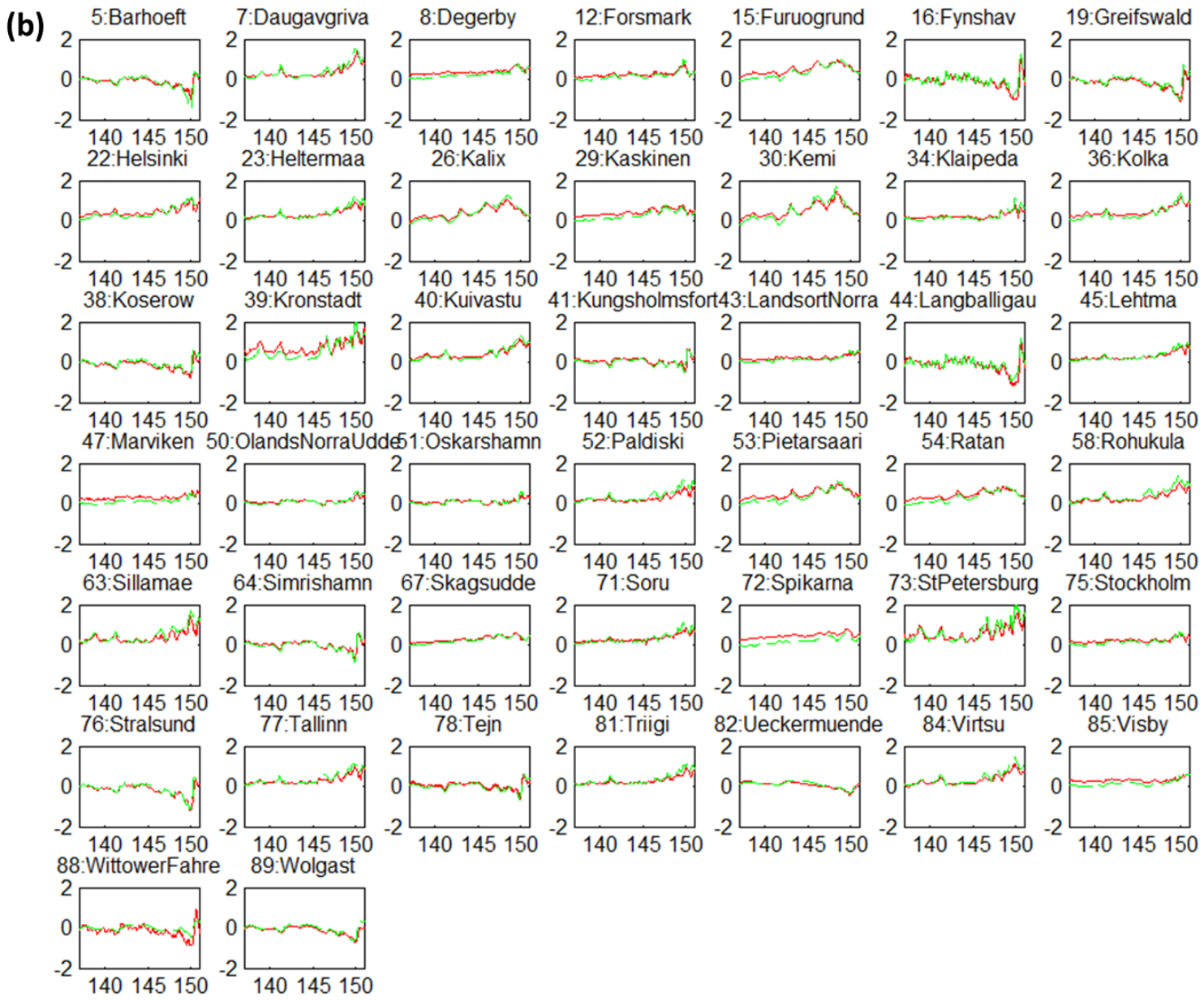
(b)
5:Barhoeft
7:Daugavgriva
8:Degerby
12:Forsmark
15:Furuogrund
16:Fynshav
19:Greifswald
22:Helsinki
23:Heltermaa
26:Kalix
29:Kaskinen
30:Kemi
34:Klaipeda
36:Kolka
38:Koserow
39:Kronstadt
40:Kuivastu
41:Kungsholmsfort
43:LandsortNorra
44:Langballigau
45:Lehtma
47:Marviken
50:OlandsNorraUdde
51:Oskarshamn
52:Paldiski
53:Pietarsaari
54:Ratan
58:Rohukula
63:Sillamae
64:Simrishamn
67:Skagsudde
71:Soru
72:Spikarna
73:StPetersburg
75:Stockholm
76:Stralsund
77:Tallinn
78:Tejn
81:Triigi
82:Ueckermuende
84:Virtsu
85:Visby
88:WittowerFahre
89:Wolgast
2
0
-2
140 145 150

Fig. A2

(c)

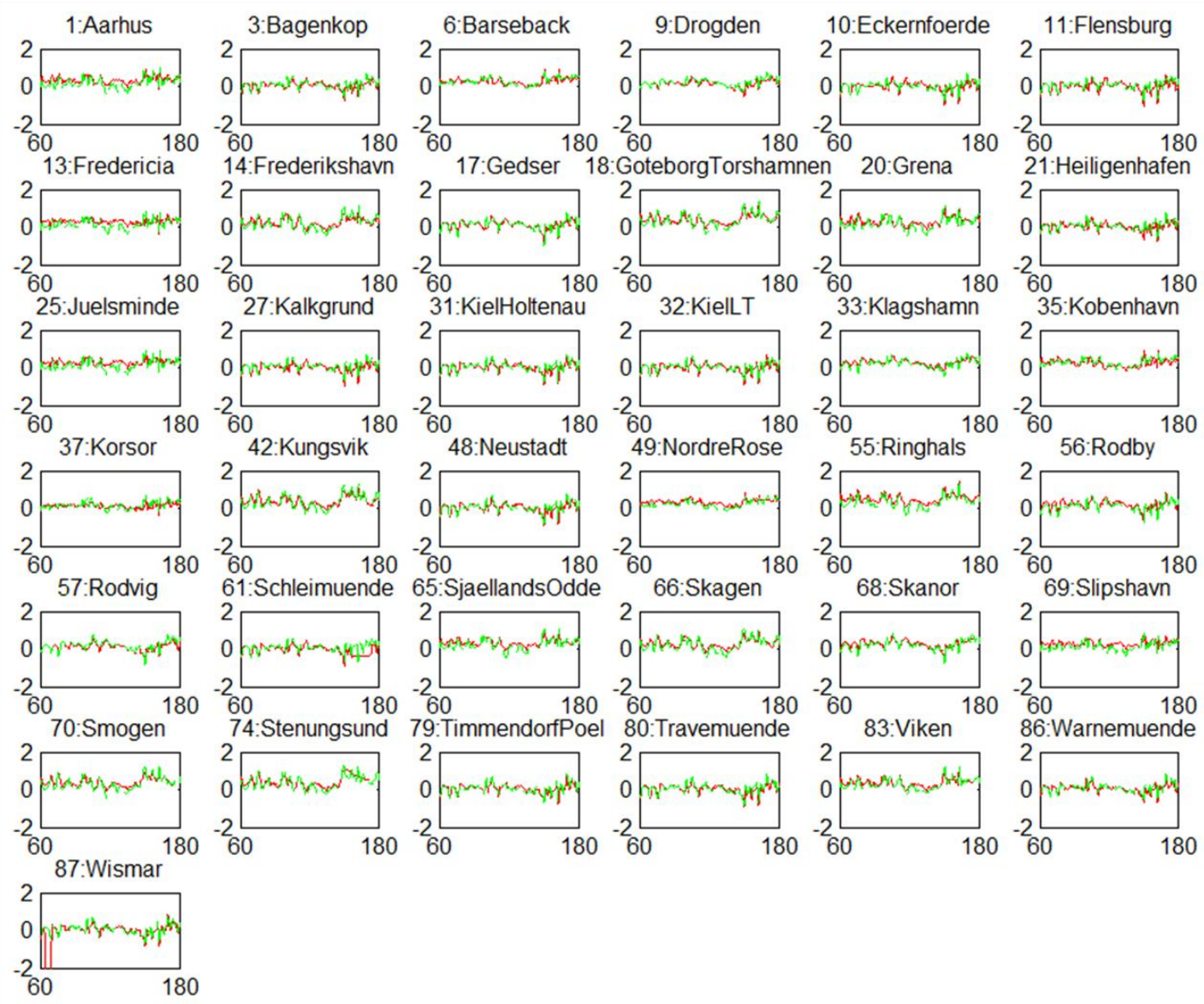
1:Aarhus
3:Bagenkop
6:Barseback
9:Drogden
10:Eckernfoerde
11:Flensburg
13:Fredericia
14:Frederikshavn
17:Gedser
18:GoteborgTorshamnen
20:Grena
21:Heiligenhafen
25:Juelsminde
27:Kalkgrund
31:KielHoltenau
32:KielLT
33:Klagshamn
35:Kobenhavn
37:Korsor
42:Kungsvik
48:Neustadt
49:NordreRose
55:Ringhals
56:Rodby
57:Rodvig
61:Schleimuende
65:SjaellandsOdde
66:Skagen
68:Skanor
69:Slipshavn
70:Smogen
74:Stenungsund
79:TimmendorfPoel
80:Travemuende
83:Viken
86:Warnemuende
87:Wismar
2
0
-2
60
180

Fig. A2

(d)

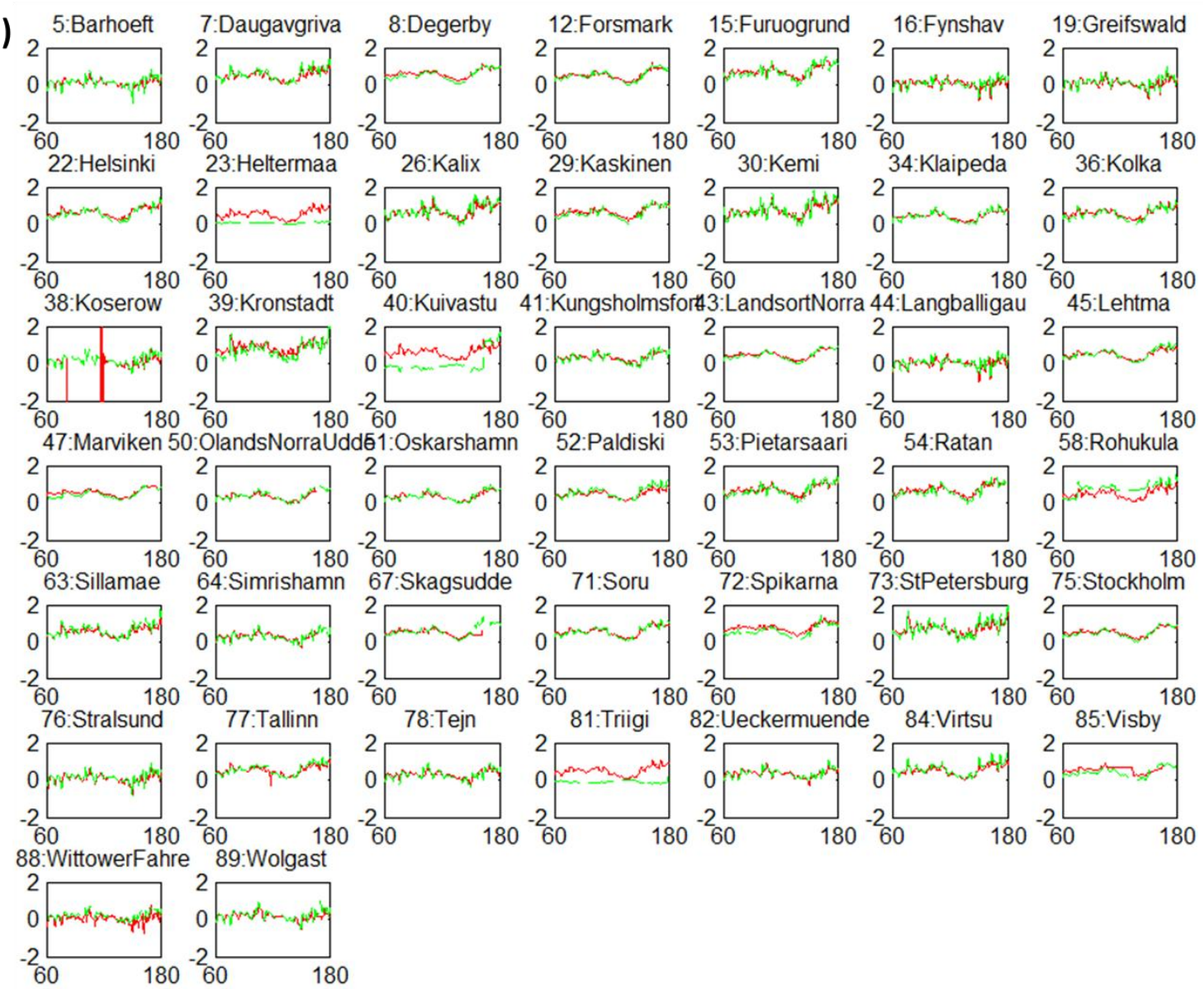
5:Barhoeft
7:Daugavgriva
8:Degerby
12:Forsmark
15:Furuogrund
16:Fynshav
19:Greifswald
22:Helsinki
23:Heltermaa
26:Kalix
29:Kaskinen
30:Kemi
34:Klaipeda
36:Kolka
38:Koserow
39:Kronstadt
40:Kuivastu
41:Kungsholmsfort
43:LandsortNorra
44:Langballigau
45:Lehtma
47:Marviken
50:OlandsNorraUdde
51:Oskarshamn
52:Paldiski
53:Pietarsaari
54:Ratan
58:Rohukula
63:Sillamae
64:Simrishamn
67:Skagsudde
71:Soru
72:Spikarna
73:StPetersburg
75:Stockholm
76:Stralsund
77:Tallinn
78:Tejn
81:Triigi
82:Ueckermuende
84:Virtsu
85:Visby
88:WittowerFahre
89:Wolgast
2
0
-2
60
180

Fig. A2